Electronic Supplementary Material (ESI) for Nanoscale.

Water soluble and bay functionalized perylenediimide derivatives – Correlating aggregation and excited state dynamics

K. Dirian,[a,+] S. Bauroth,[a,+] A. Roth,[a] Z. Syrgiannis,[b] F. Rigodanza,[b] M. Burian,[c] H. Amenitsch, D.I. Sharapa,[a] [c] M. Prato[b, d, e], T. Clark[a] and D.M. Guldi[a*]

Supplementary Information

1. Steady state absorption spectroscopy

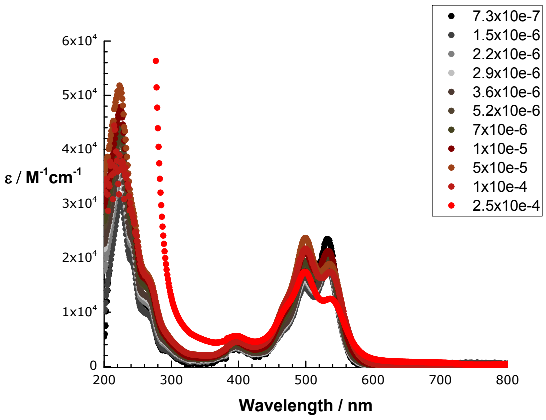

Figure S1: Left: Extinction spectra of ***1*** *with different concentrations from 7.3x10^{-7} M (light grey) to 2.5x10^{-4} M (red) recorded in H_2O.*

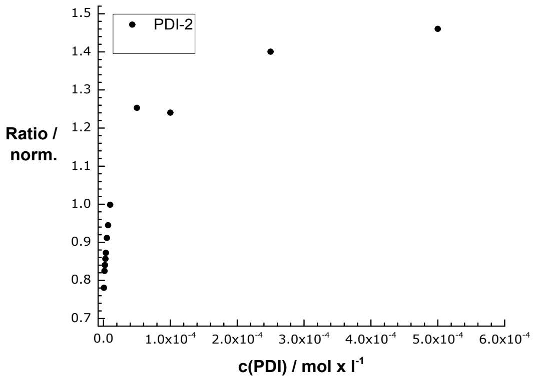

Figure S2: Relative intensities of the maxima at 498 and 532 nm of ***1*** *shown as function of concentration.*

2. Molecular modelling

To investigate the structure and binding energies of the aggregates a variety of calculation methods was used. Initial Dreiding Forcefield calculations were performed in the gas phase, optimizing the monomer of 1 and performing rigid torsion scans along β and δ (see Figure S3). For the energetically most favored structures, β and δ were determined to be 90° and 180°. The trans- conformation, where both ethylamine groups are on opposite sides of the PDI-plane, is predicted to be 2.5 kcal mol^{-1} better stabilized than the cis- conformation. Turning to the aggregates, first the dimer was studied with the Forcefield approach using 100 stimulated annealing cycles (mid cycle temperature 500 K, Berendsen thermostat), followed by optimization. Based on the energetically most favored structure, we constructed an aggregate consisting of 20 monomers and again annealed and optimized them under the same conditions. All these initial calculations were performed in the gas phase using Forcite package included in BIOVIA Materials Studio 2016.

Based on the structures obtained by this pre-screening, two approaches were used to study the aggregation. Within the first approach, the mono-, di-, tri-, tetra- and pentamer were optimized using the PBE0 method with cc-pVDZ basis including Grimme GD3 dispersion correction and PCM solvation of water. Single point calculations and rigid scans along in various solvent environments were performed to elucidate the impact of solvation on the aggregation. Furthermore, the dimer of 1 was used to perform a rigid scan along the distance between the two monomer units in different solvent environments. In each case, the energies were compared by determining the dimerization energies according to equation (i), where n represents the number of monomers in the aggregate.

$$E_D = \frac{\left(E_n - n \cdot E_1\right)}{n-1} \qquad (i)$$

Different diasteriomers of the di- and trimer were optimized and compared energetically. As shown in Figure S6 A, 180 degree rotation of β results in a 2.25 kcal mol^{-1} less stable cis- conformation of the dimer. Due to low C1 symmetry group in trans- conformation (C2 in cis- conformation) and the chirality the monomer, diasteriomers of the dimer and trimer (Figure S6 B and C) were optimized and found to be 1.0 and 3.2 kcal mol^{-1} less stable than the predicted global minima (Figure S4).

For comparison with the experimental absorption data, time dependent PBE0 calculations were performed including 30 singlet and 30 triplet excited states (Figure S10-S11). All DFT results were obtained using the Gaussian09 software package with default settings.

In a second approach, force field molecular dynamic calculations were used to study stability under solvated conditions. At the very beginning an aggregate consisting of 20 monomers was placed in rectangular box (buffer – 10 Å) using *leap* program of AmberTools[i] and box was filled with TIP3P water[ii] (*solvatebox*). 40 chloride ions were added to neutralize the system using *addion2*. GAFF[iii] parameters were used for solute and charges in each solute molecule were taken from "*HF/6-31G* SCF=tight Pop=MK iop(6/33=2) iop(6/42=6)*" single point Gaussian09 calculation of monomer (optimized as specified above) that is a canonical way for charge generation. 500 step minimization (prior to MD) was performed with cut off range for the long range non-bonded interactions of 12Å. After that short equilibration (1 ns, not used in further analysis) and 10 ns molecular dynamic simulation were performed using *sander* and *pmemd* tools of Amber16. Langevin thermostat (NTT=3) was used to maintain the temperature of the system at 300 K during 500000 steps (2 fs time step). 10 Å cutoff was used during MD. Density of equilibrated system stays at 1.04 g/cm^3 during the whole MD simulation, temperature deviation never overcame 5 degrees.

Snapshots, taken every 500ps, were used to do AM1 CIS single point calculations including an active space of 100 in water PCM solvation. The data were scaled using the slope and intercept of the correlation between experimental and calculated data of the initially calculated Monomer.

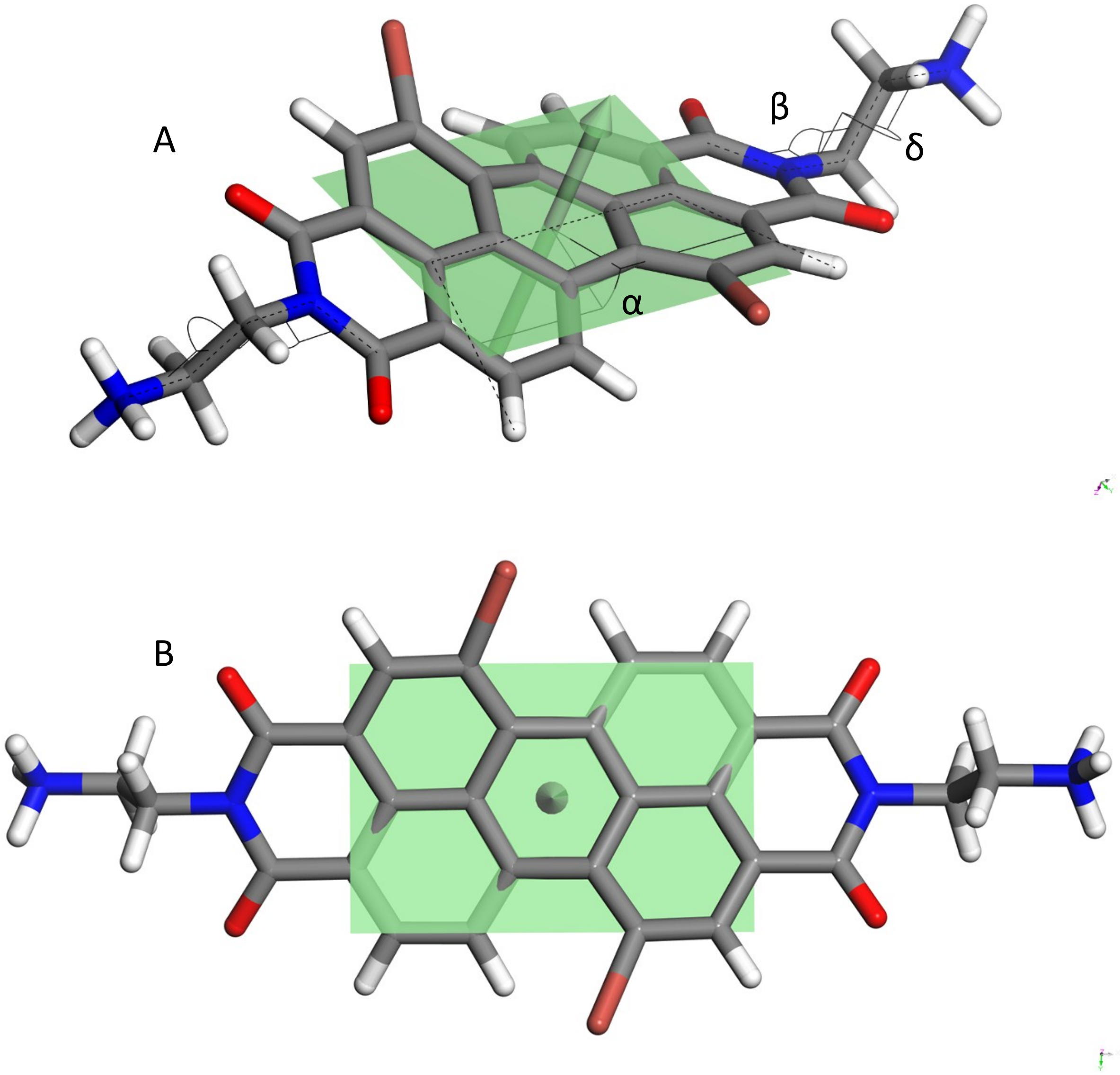

Figure S3: Optimized monomer geometry obtained from PBE0/cc-pVDZ calculation including water PCM solvation. A indicates the bay twist angle α, and the two torsion angles β and δ.

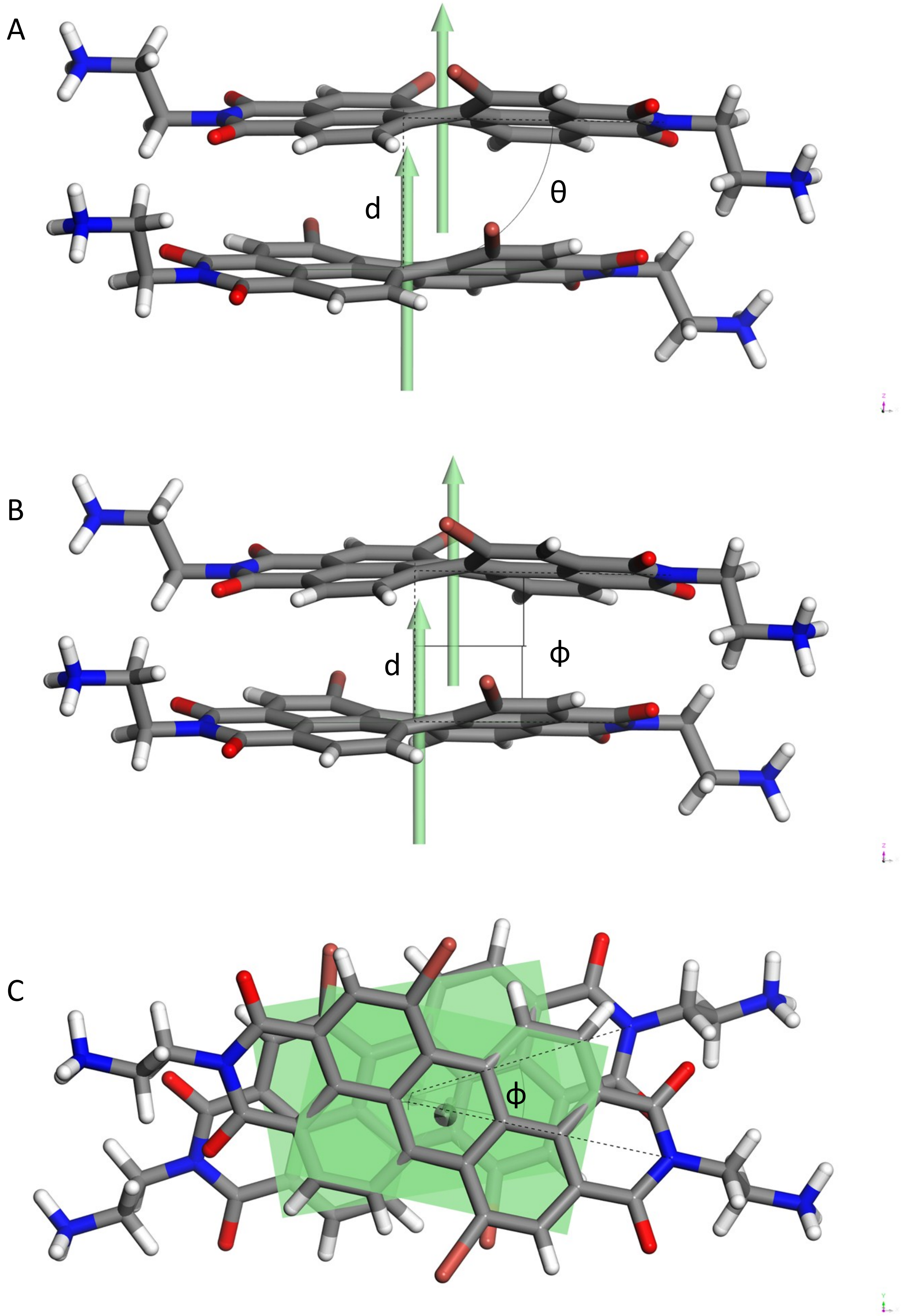

Figure S4: Optimized dimer geometry obtained from PBE0/cc-pVDZ calculations including water PCM solvation: A shows the distance d and the slip angle θ, while B and C show the torsion angle ϕ.

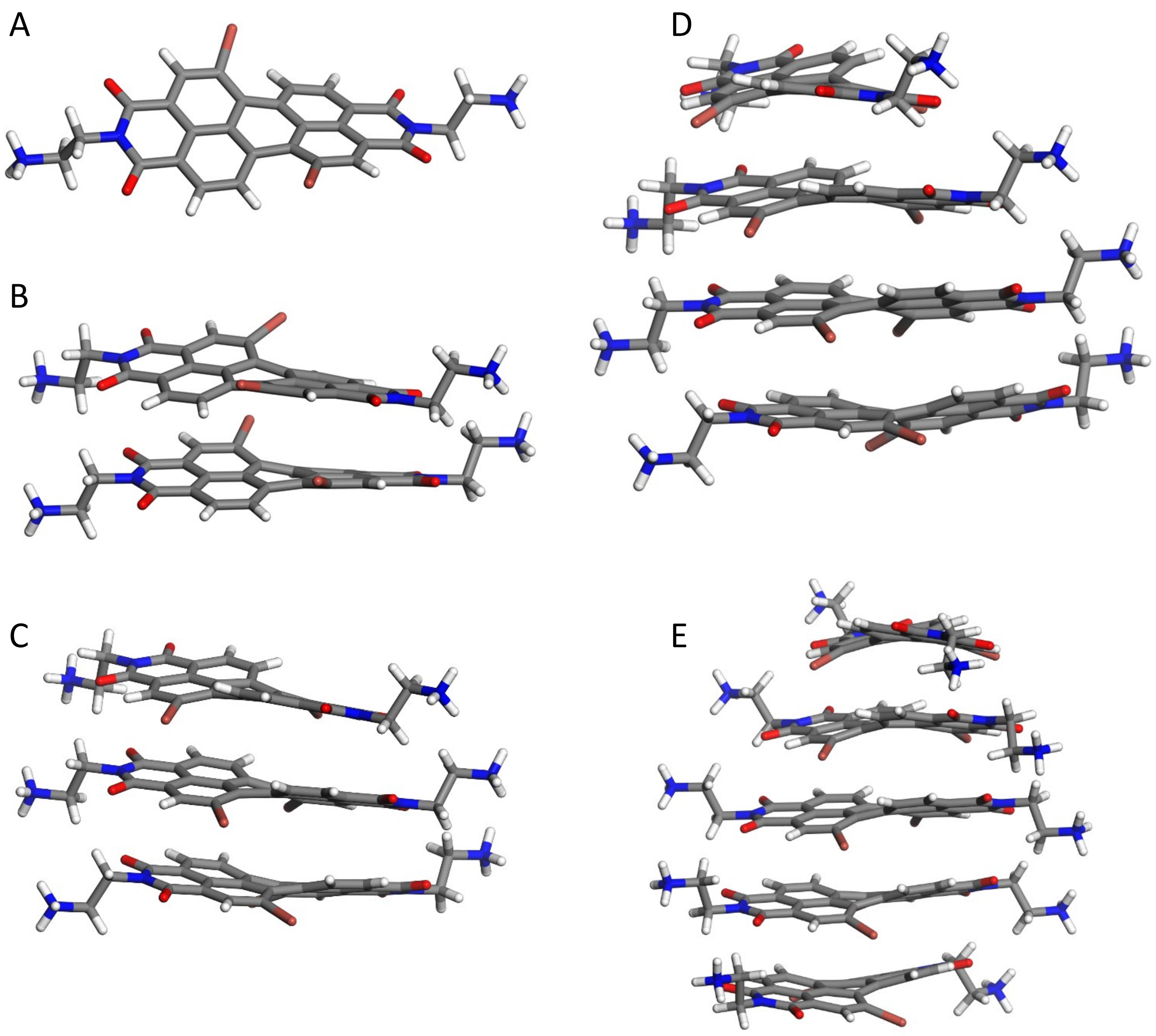

Figure S5: Optimized geometries obtained from PBE0/cc-pVDZ calculations including water PCM solvation of the mono- (A), di- (B), tri- (C), tetra- (D), and pentamer (E)

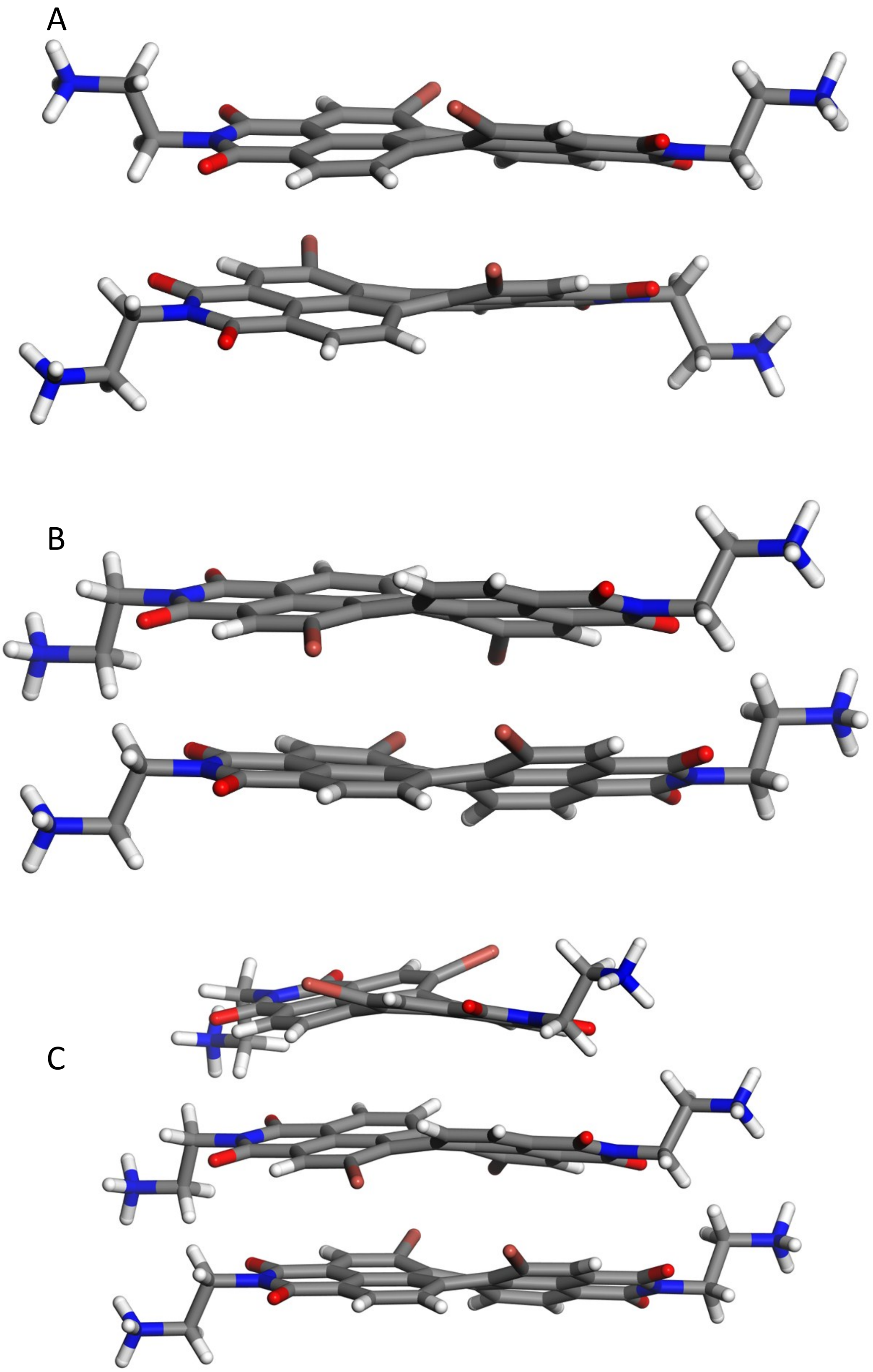

Figure S6: Optimized local minima geometries of different stereoisomers obtained from PBE0/cc-pVDZ calculations including water PCM solvation. The cis- conformation of the dimer (A) was predicted to be 2.3 kcal mol^{-1} less stable than the trans- conformation – Figure S4. B and C show the optimized local minima for the chiral stereoisomers of the dimer and trimer, respectively. They are predicted to be 1.0 and 3.2 kcal mol^{-1} less stable than the isomers shown in Figure S5.

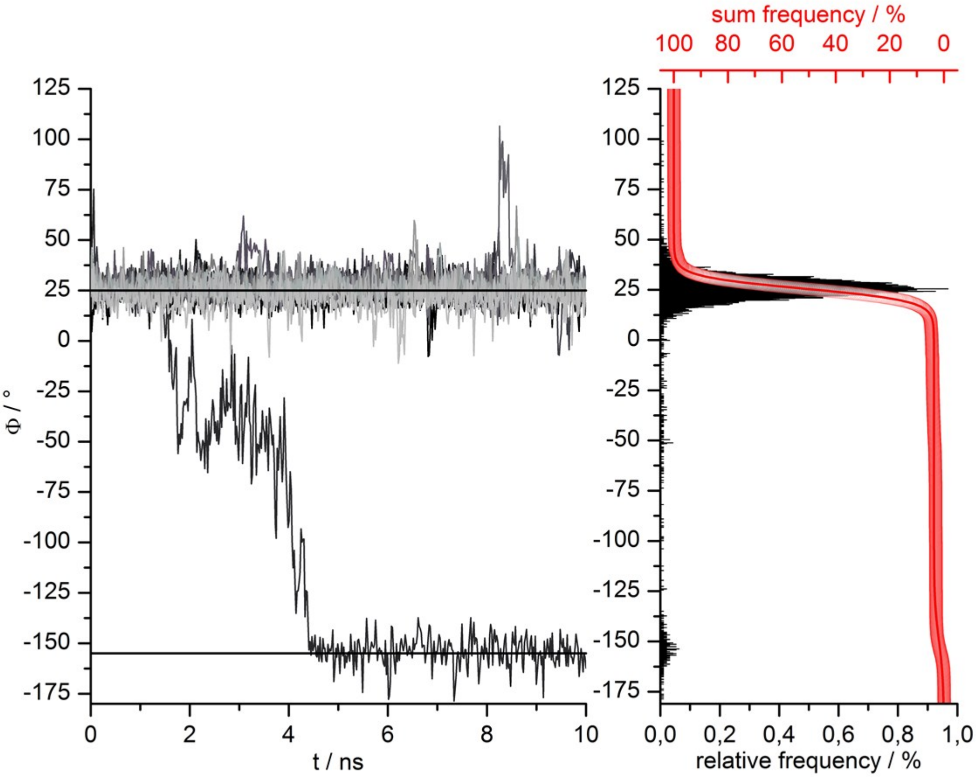

Figure S7: left: Torsion evolution of Φ during MD-simulation of 10 ns in water solvation. right: relative frequency distribution (0.1 ° bin size, black) and sum frequency distribution (red)

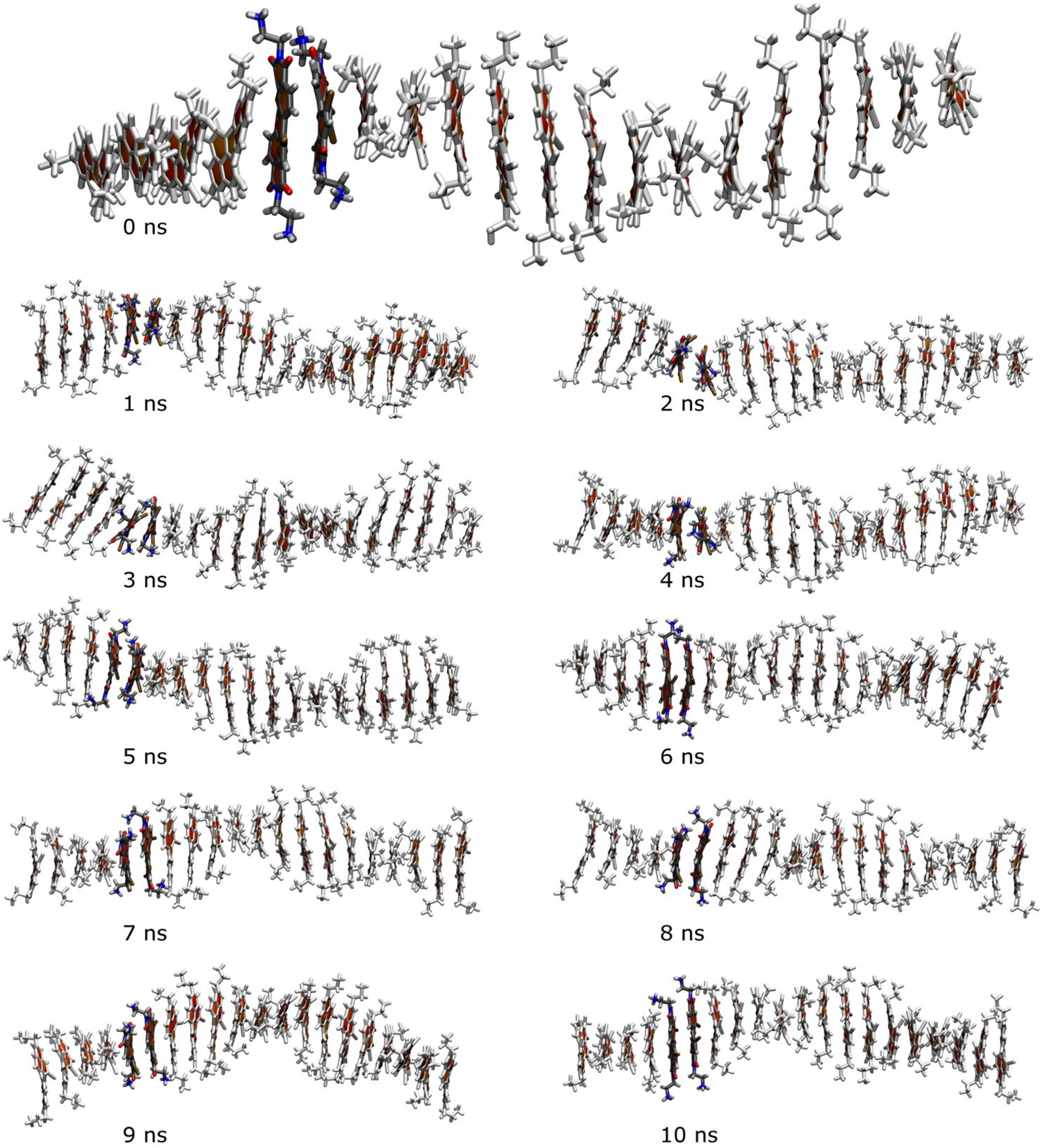

Figure S8: Geometry snapshots obtained by MD calculation with 1 ns time delay. 180° rotation around dihedral twist angle φ between PDI five and six (colored) was noted.

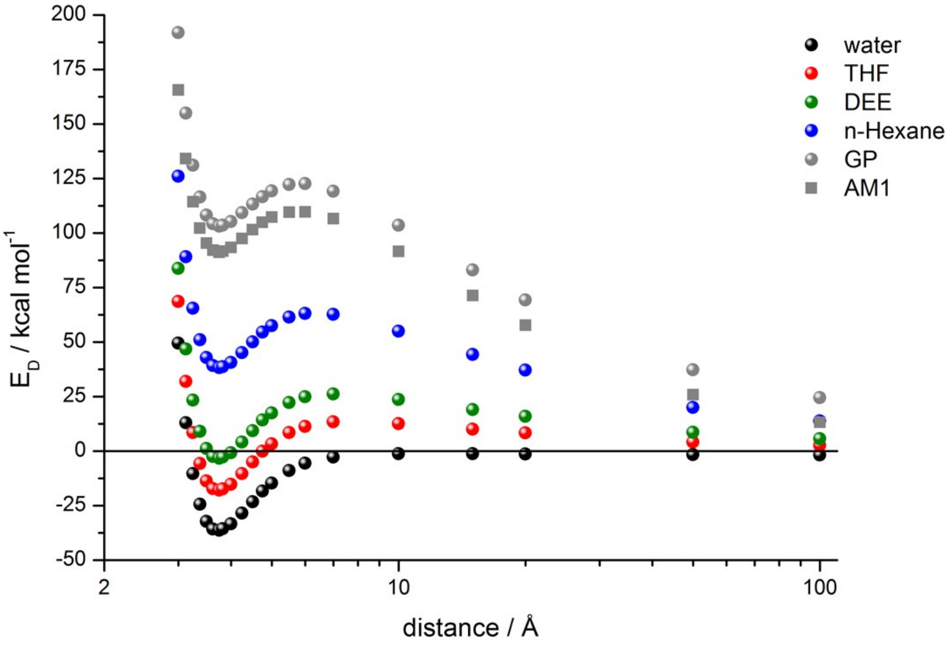

Figure S9: Distance dependences of the dimerization energy obtained from gas phase AM1 gas phase calculations (grey squares) as well as PBE0/cc-pVDZ calculations (dots) in the gas phase (grey) and including PCM solvation of water (black), THF (red), diethylether (green), and n-hexane (blue).

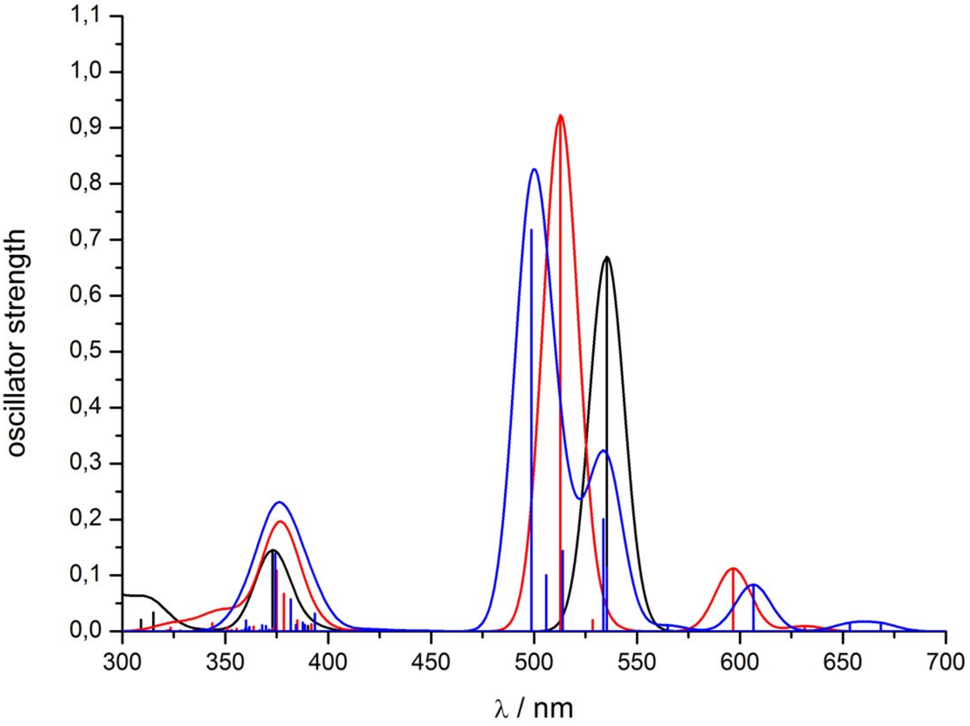

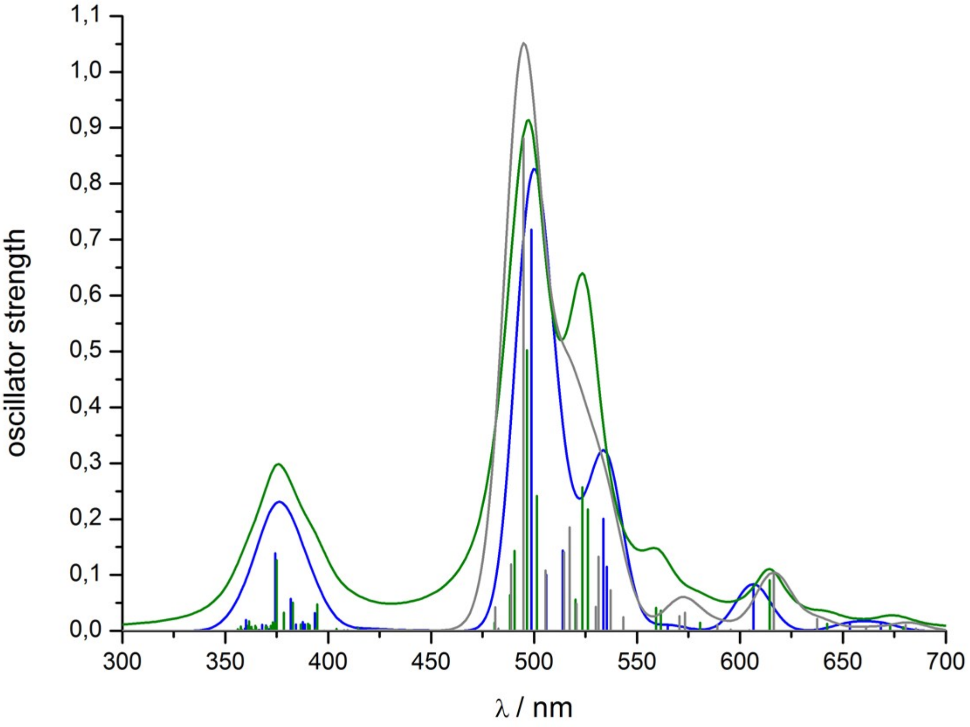

Figure S10: Predicted absorption spectra for monomer (black), dimer (red), trimer (blue), tetramer (green),and pentamer (grey) obtained from TD-PBE0/cc-pVDZ calculations including PCM water solvation. The spectra were obtained by the sum of gauss distributions with 10 nm full-width half-maximum.

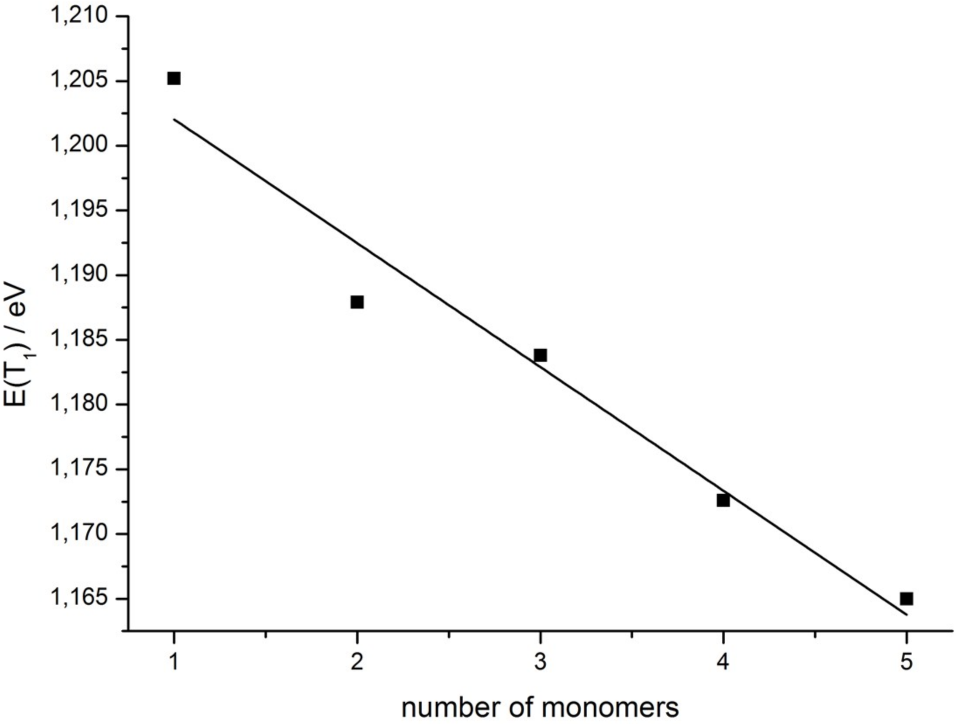

Figure S11: Predicted singlet triplet energy gap as a function of aggregate size.

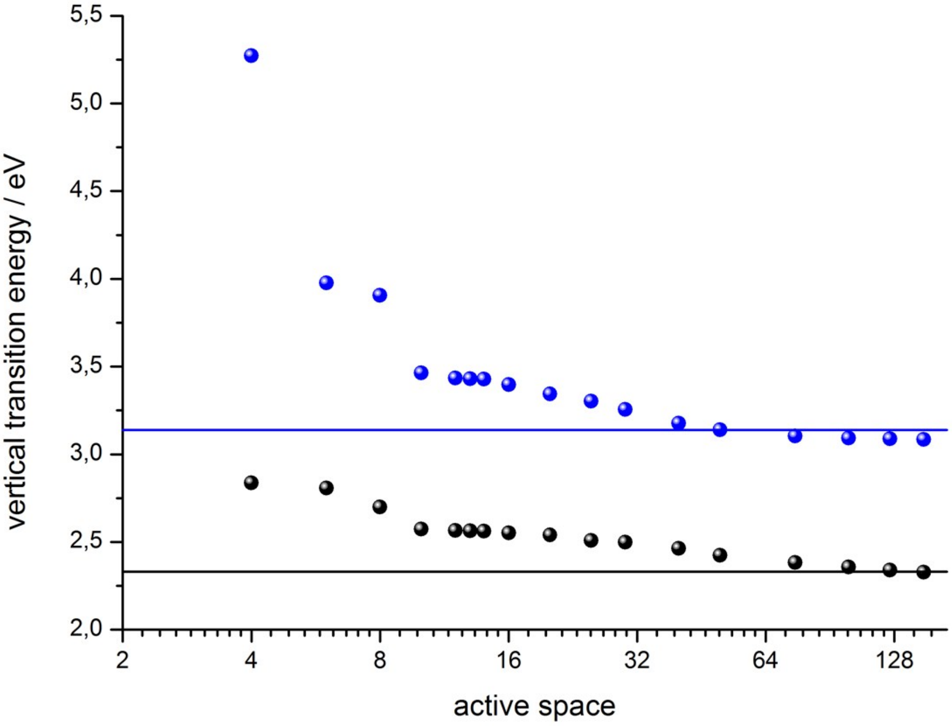

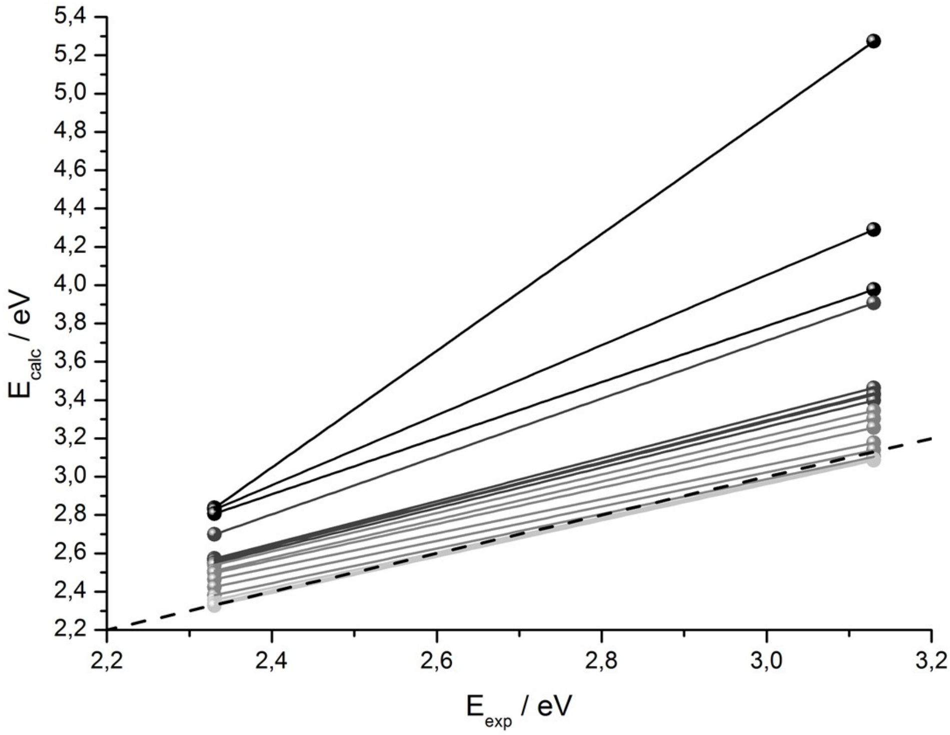

Figure S12: Top: AM1 CIS predicted vertical transition energies of the monomer for S0 to S1 (black dots) and S0 to S2 (blue dots) in dependence of the active space (AS). Experimental values (lines) are taken from the absorption maxima. Bottom: Correlation of predicted and experimental values for an AS=4 (black) to AS=150 (light grey). The dotted line resembles perfect correlation. The slope and intercept was used to correct the 20mer CIS calculation.

.

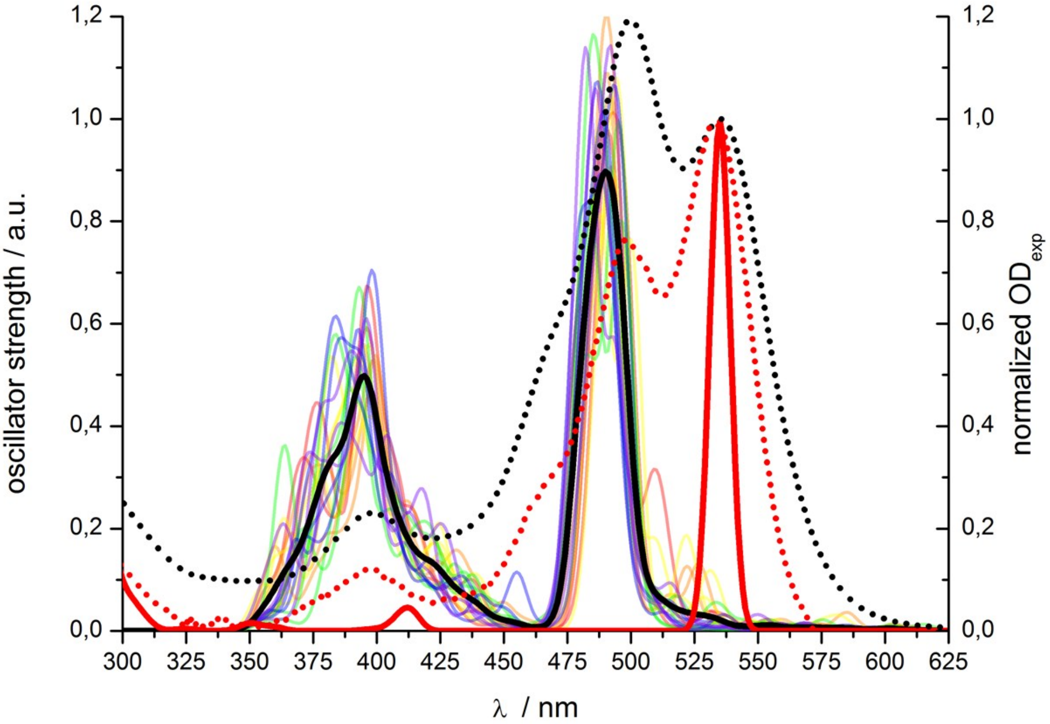

Figure S13: Corrected AM1 CIS predicted absorption spectra (AS=100) of 20mer for 21 structures during MD simulation (transparent rainbow colors). Structures were taken every 500ps ranging from 0 ns (light red) to 10 ns (light purple). Spectra were fitted with 8 nm FWHM Gaussian distribution and averaged (black line). Predicted monomer (red line, AS=150) and normalized experimental absorption spectra at 7.3 x 10^{-7} M (red dots) and 5 x 10^{-4} M (black dots) are given as reference.

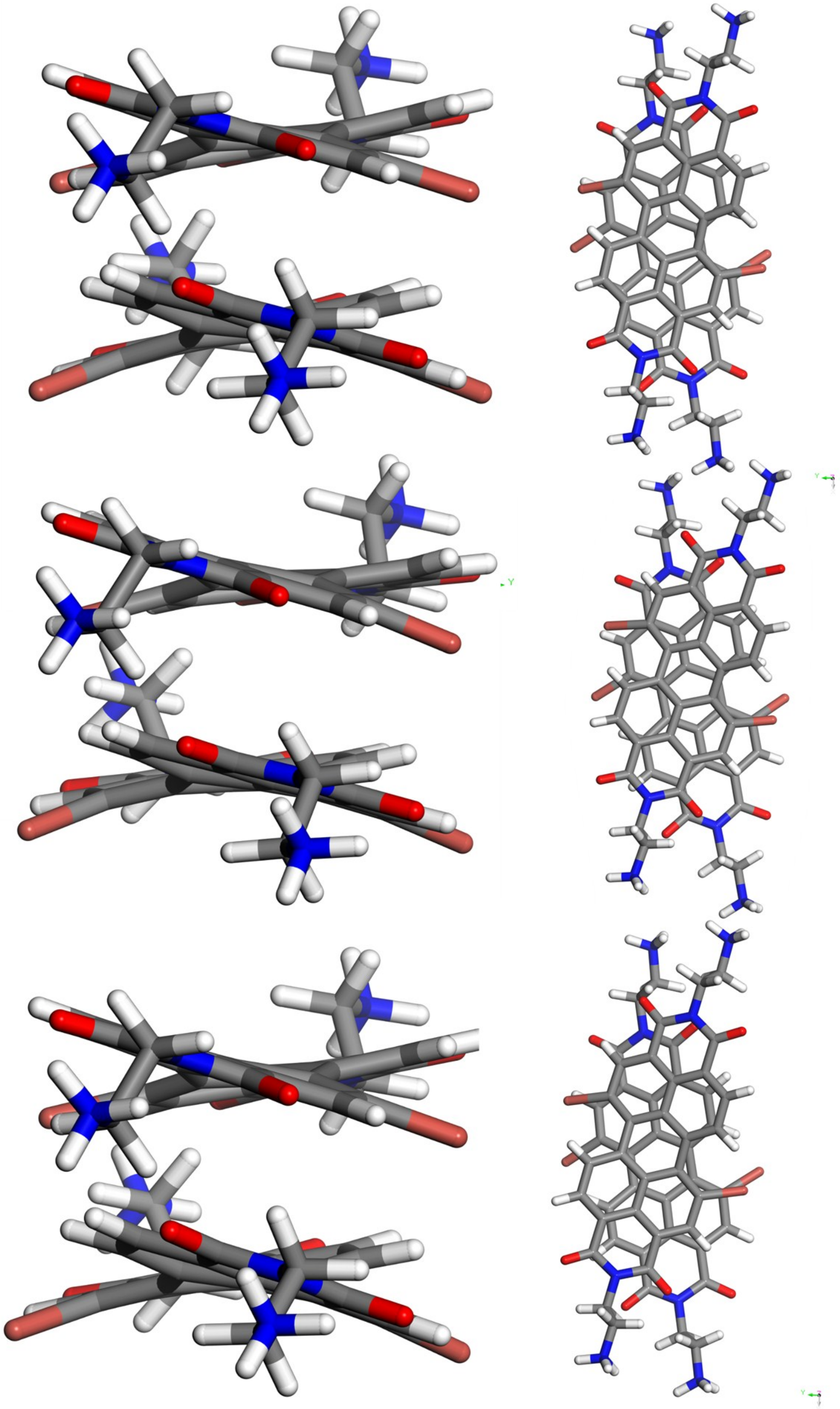

Figure S14: DFT Optimized geometries for reduced dimer (top), dimer (middle) and oxidized dimer (bottom)

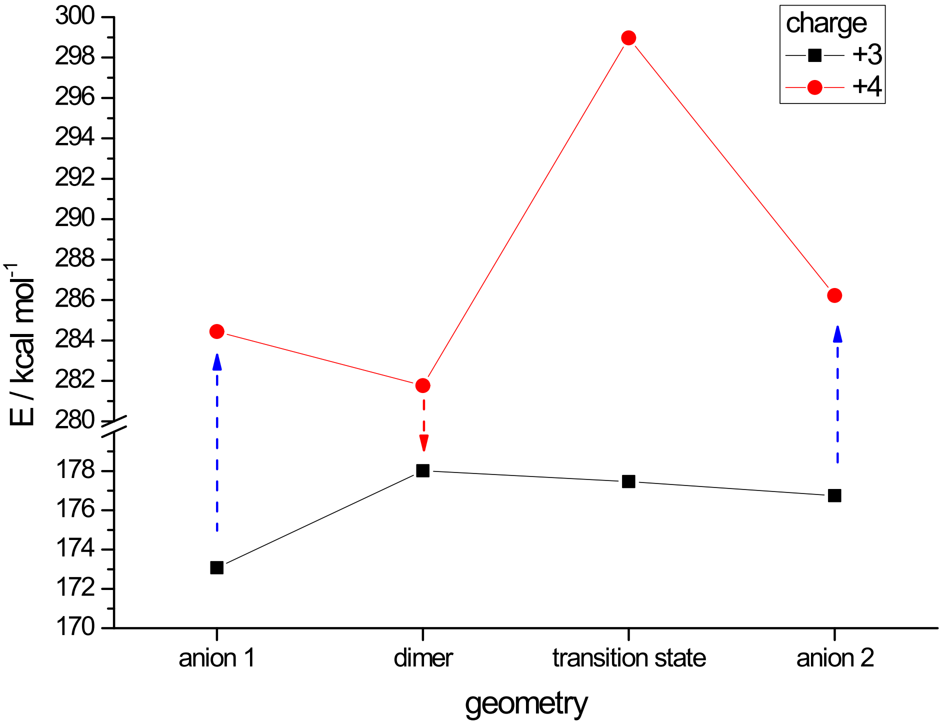

Figure S15: AM1 predicted heat of formations of the two reduced dimer structures (anion1 and anion 2), the dimer, and the transition state in dependence of the system charge. Reduction and re-oxidation are displayed with red and blue arrows.

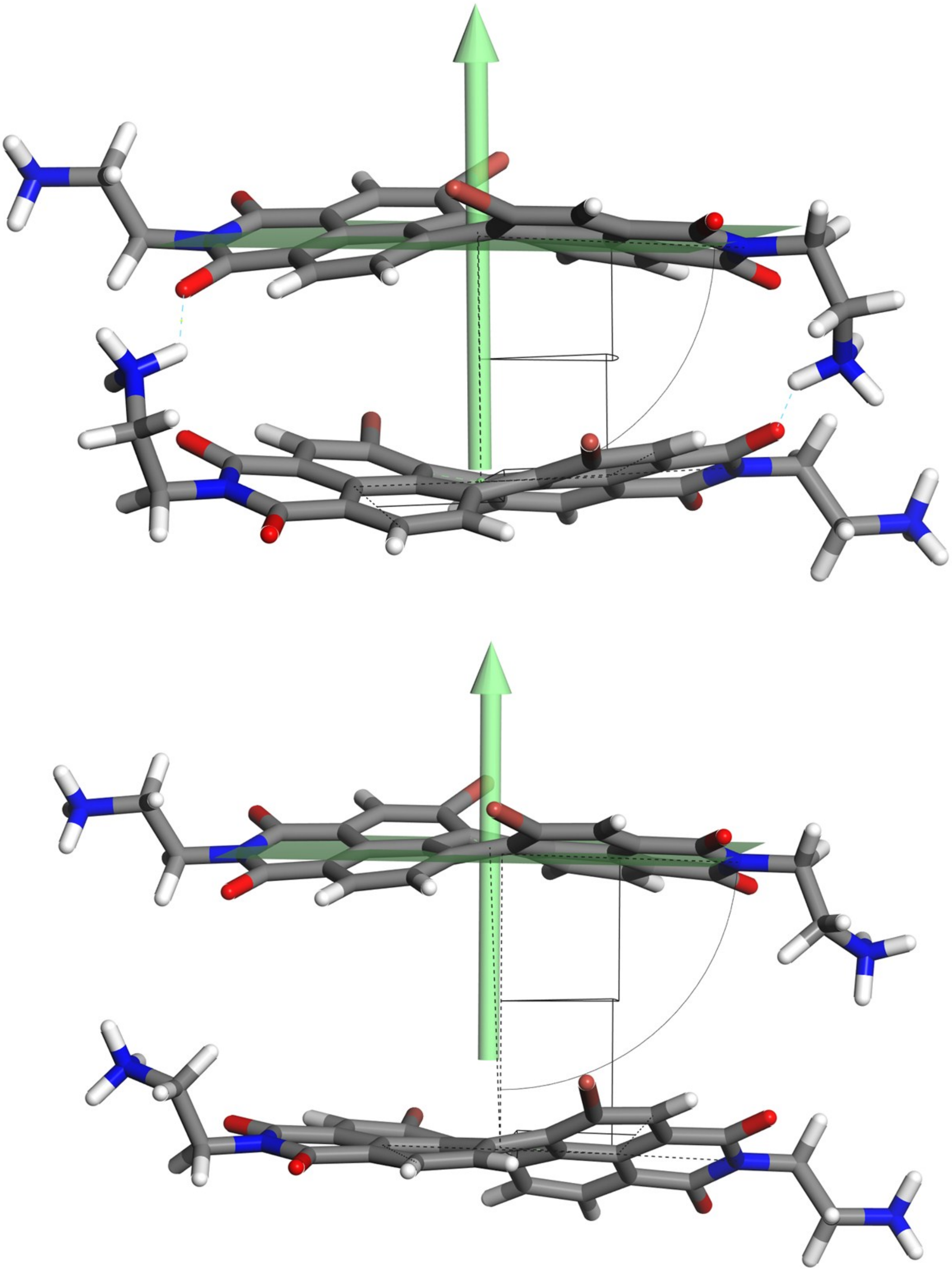

Figure S16: AM1 optimized geometries for the local minima structure of the reduced dimer (top) and for the transition state, based on four times positive charge (bottom)

3. Atomic force (AFM) and transmission electron microscopy (TEM)

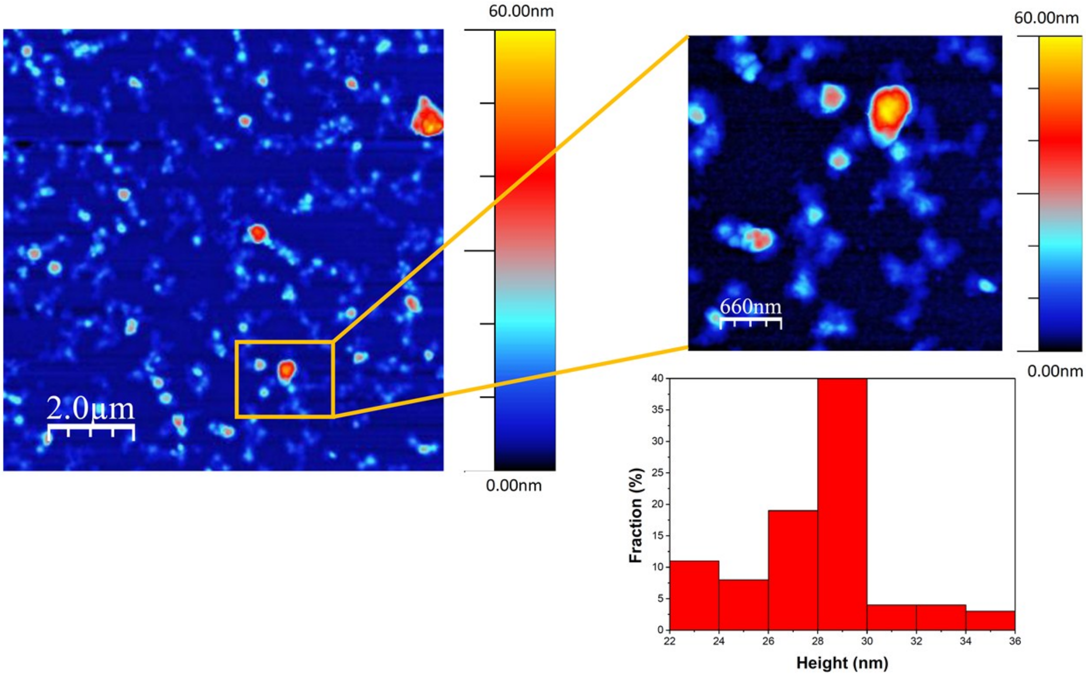

*Figure S17: AFM image, zoom in and statistical height distribution of **1** on a mica substrate.*

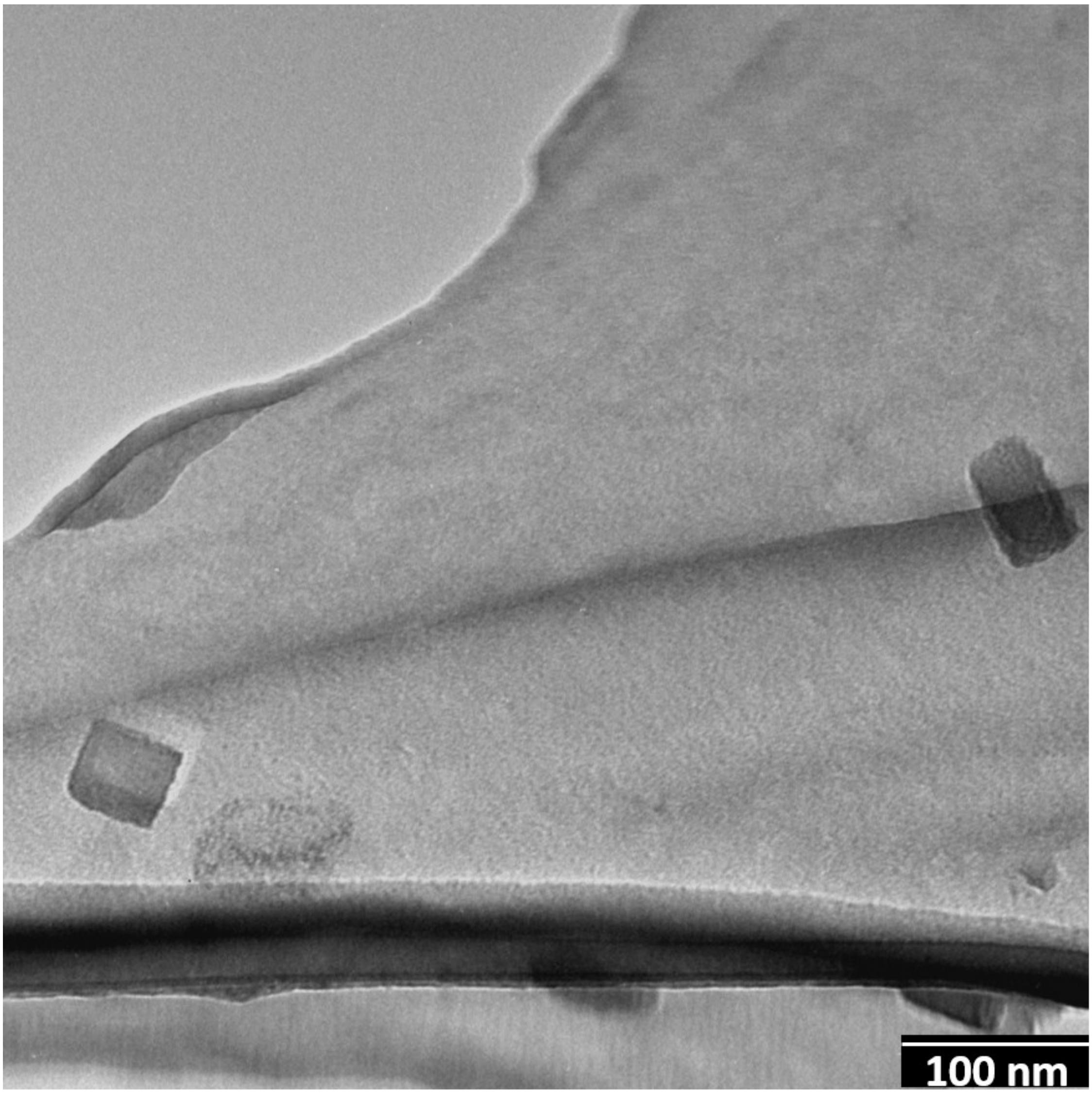

*Figure S18: TEM image of a 5 x10^{-4} M solution of **1** dropcasted and dried on a lacey carbon coated copper grid.*

4. Steady state emission spectroscopy

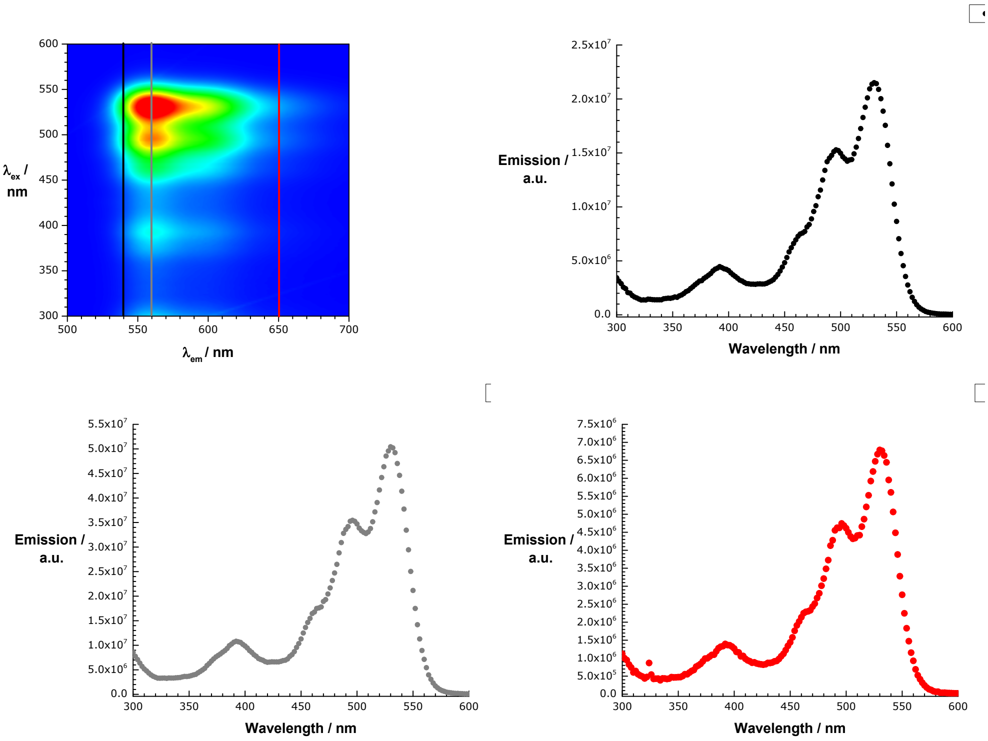

*Figure S19: Top left: 3D excitation/emission plots of **1** (1x10^{-5} M) in H_2O. Top right: Corresponding excitation spectrum recorded at λ_{em} = 540 nm. Bottom left: Corresponding excitation spectrum recorded at λ_{em} = 560 nm. Bottom right: Corresponding excitation spectrum recorded at λ_{em} = 650 nm.*

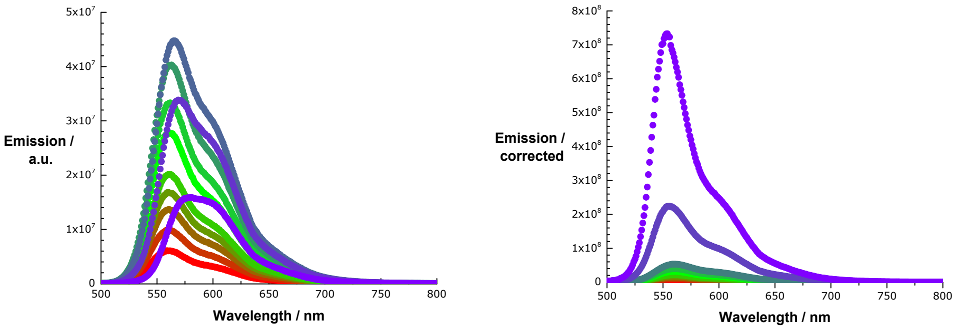

Figure S20: Left: Emission spectra of ***1*** *obtained upon 480 nm excitation with different concentrations from 7.3x10*$^{-7}$ *(red) to 10*$^{-4}$ *M (blue) recorded in* H_2O *without correction for inner filter effects. Right: Corresponding spectra after correction for inner filter effects.*

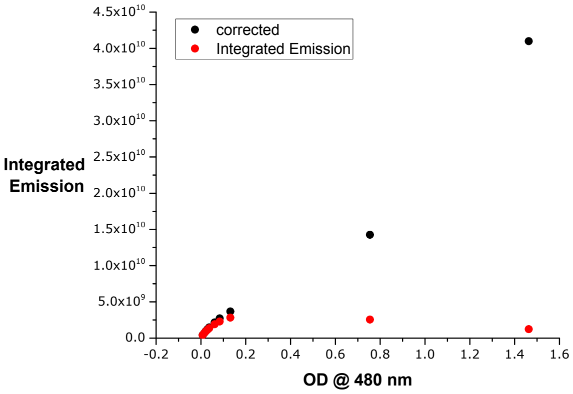

Figure S21: Plot of the integrated emission of ***1*** *versus the optical density at the excitation wavelength (480 nm) without (red cycles) and with correction for inner filter effects (black cycles).*

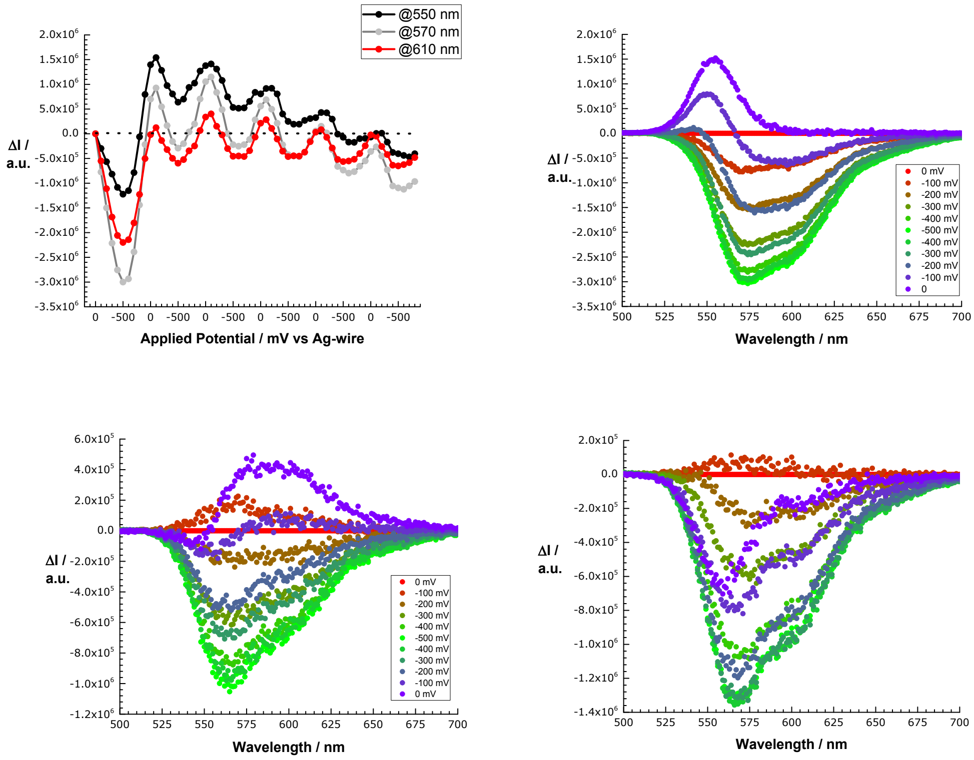

Figure S22: Top left: Correlation of the differential intensities obtained from reduction and reoxidation of ***1*** *(1x10^{-4}M, H_2O, 0.05M Na_2SO_4) in the course of several electrochemical sweeps. Top right/bottom left/bottom right: Corresponding differential emission spectra of* ***1*** *recorded during the first three electrochemical cycles from 0 mV (red) to -500mV (green) followed by reoxidation (blue).*

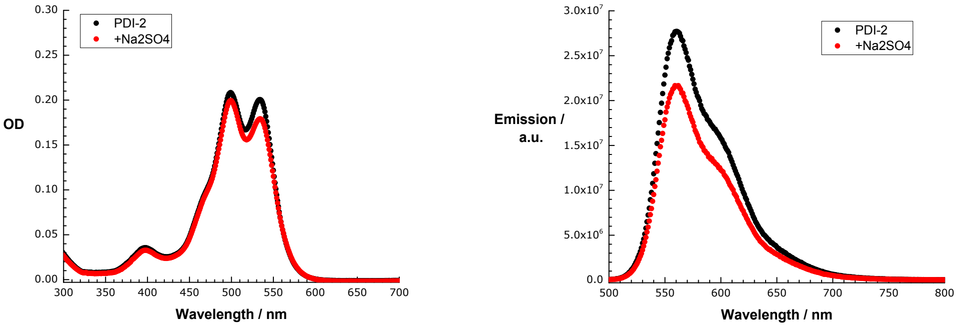

*Figure S23: Left: UV/Vis absorption spectra of **1** (1x10^{-5}M) in absence (black) and presence (red) of Na_2SO_4 in H_2O. Right: Corresponding emission spectra of **1** (1x10^{-5}M) in absence (black) and presence (red) of Na_2SO_4 in H_2O upon 480 nm excitation.*

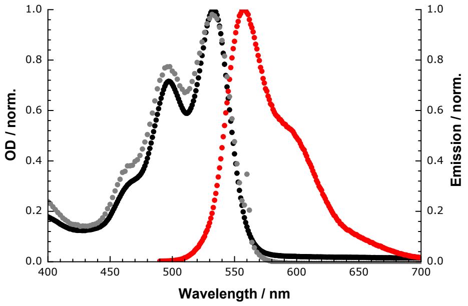

Figure S24: Bottom: Combined absorption (black), excitation (grey) and emission (red) spectra of ***1*** *($1x10^{-5}$M) in SDBS (0.5 wt%) containing H_2O. λ_{em} = 560 nm and λ_{ex} = 480 nm.*

5. Time resolved transient absorption spectroscopy

a. Femtosecond transient absorption spectroscopy

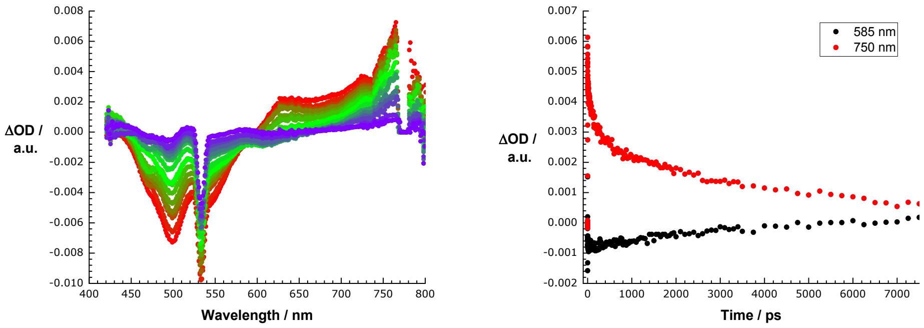

e

*Figure S25: Left: Differential absorption spectra of **1** (c=$2.5x10^{-5}$ M) in H_2O with different time delays from 2 (red) to 7500 ps (blue) obtained upon 530 nm laser excitation. Right: Time absorption profiles at 585 nm (black) and 750 nm (red) monitoring the excited state decay.*

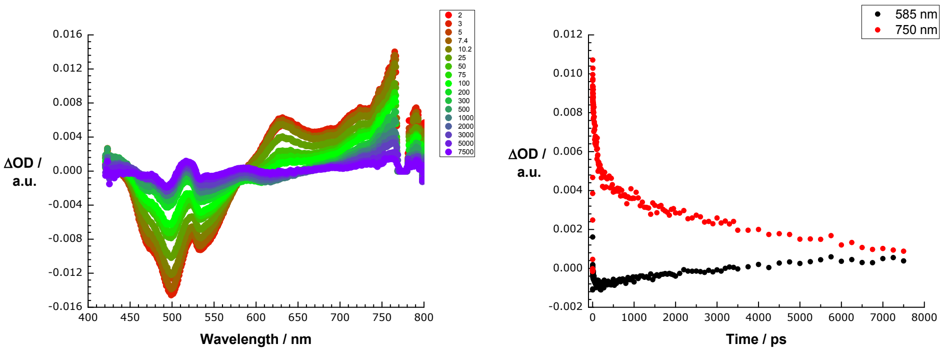

Figure S26: Left: Differential absorption spectra of ***1*** *(c=5x10^{-5} M) in H_2O with different time delays from 2 (red) to 7500 ps (blue) obtained upon 530 nm laser excitation. Right: Time absorption profiles at 585 nm (black) and 750 nm (red) monitoring the excited state decay.*

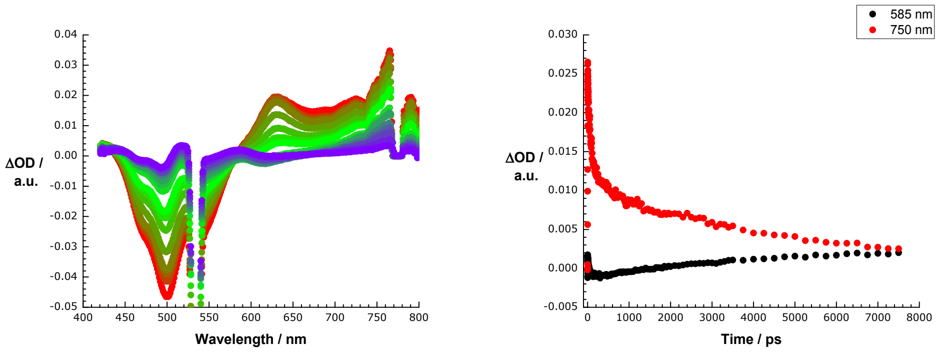

Figure S27: Left: Differential absorption spectra of ***1*** *(c=1x10^{-4} M) in H_2O with different time delays from 2 (red) to 7500 ps (blue) obtained upon 530 nm laser excitation. Right: Time absorption profiles at 585 nm (black) and 750 nm (red) monitoring the excited state decay.*

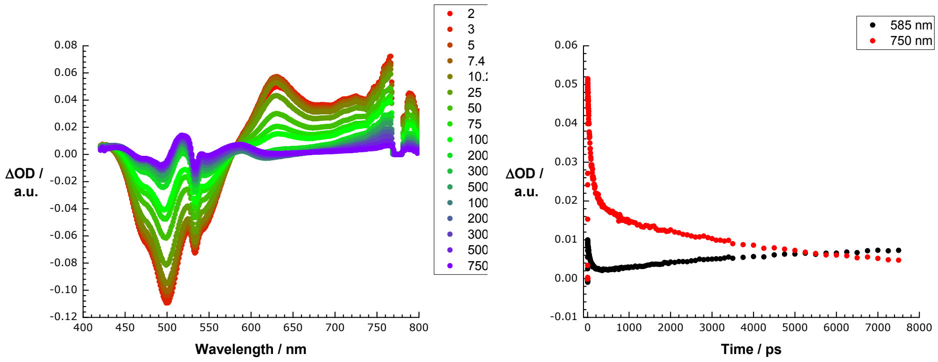

*Figure S28: Left: Differential absorption spectra of **1** (c=2.5x10^{-4} M) in H_2O with different time delays from 2 (red) to 7500 ps (blue) obtained upon 530 nm laser excitation. Right: Time absorption profiles at 585 nm (black) and 750 nm (red) monitoring the excited state decay.*

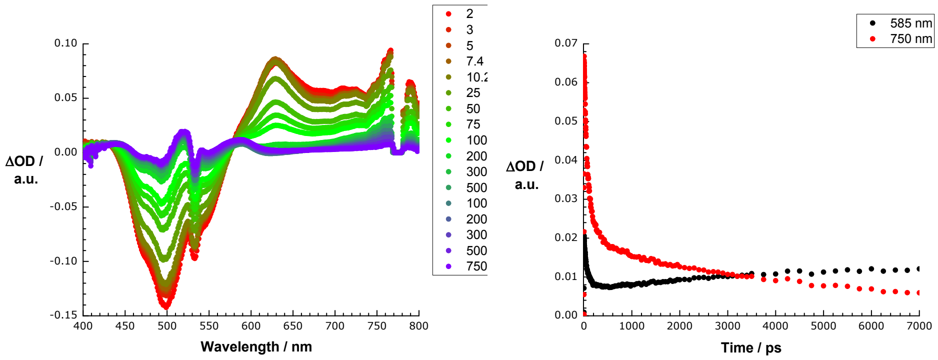

Figure S29: Left: Differential absorption spectra of ***1*** *(c=5x10^{-4} M) in H_2O with different time delays from 2 (red) to 7500 ps (blue) obtained upon 530 nm laser excitation. Right: Time absorption profiles at 585 nm (black) and 750 nm (red) monitoring the excited state decay.*

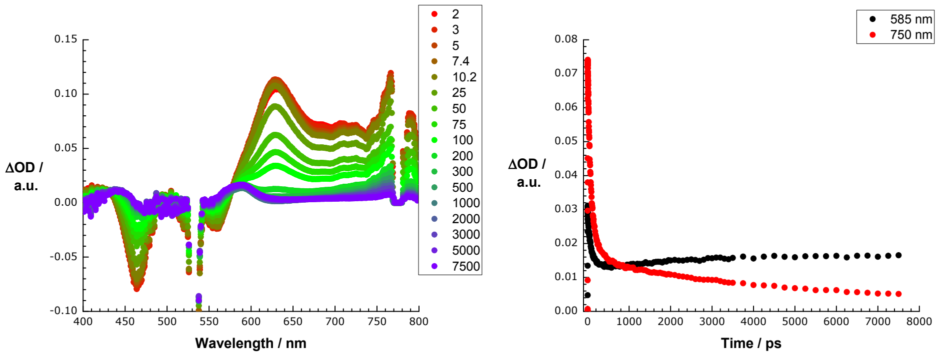

*Figure S30: Left: Differential absorption spectra of **1** (c=1x10^{-3} M) in H_2O with different time delays from 2 (red) to 7500 ps (blue) obtained upon 530 nm laser excitation. Right: Time absorption profiles at 585 nm (black) and 750 nm (red) monitoring the excited state decay.*

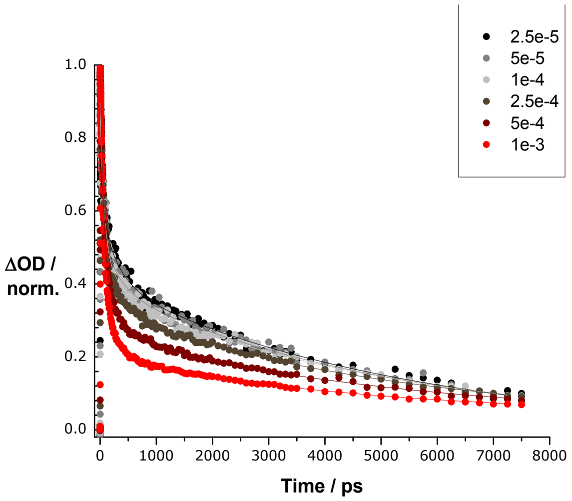

*Figure S31: Corresponding normalized time absorption profiles of **1** recorded at 750 nm with different concentrations, that is, 2.5 x 10^{-5} (black), 5.0 x 10^{-5} (dark grey), 1.0 x 10^{-4} (grey), 2.5 x 10^{-4} (light brown), 5.0 x 10^{-4} (brown), and 1.0 x 10^{-3} M (red)*

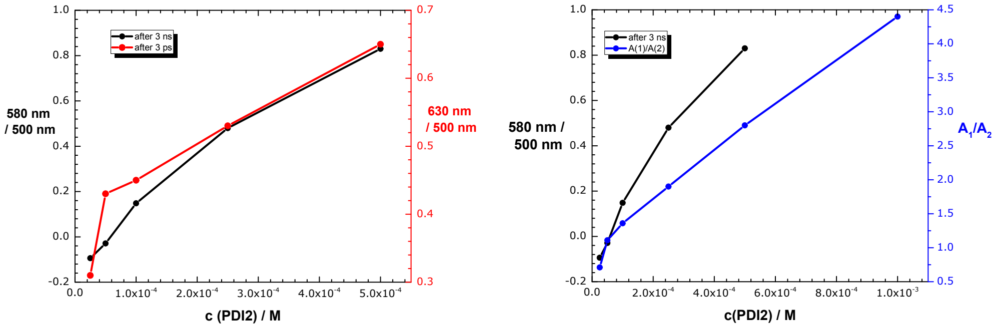

Figure S32: Left: Plot of the relative intensities of the 580/500 nm after 3ns (black) and 630/500 nm after 3ps (red) transient absorptions as a function of the concentration of ***1****. Right: Plot of the relative intensities of the 580/500 nm transient (black) and the relative amplitudes of the short lived (*A_1*) and long lived (*A_2*) kinetic components monitored at 750 nm as function of the concentration of* ***1****.*

b. Nanosecond transient absorption spectroscopy

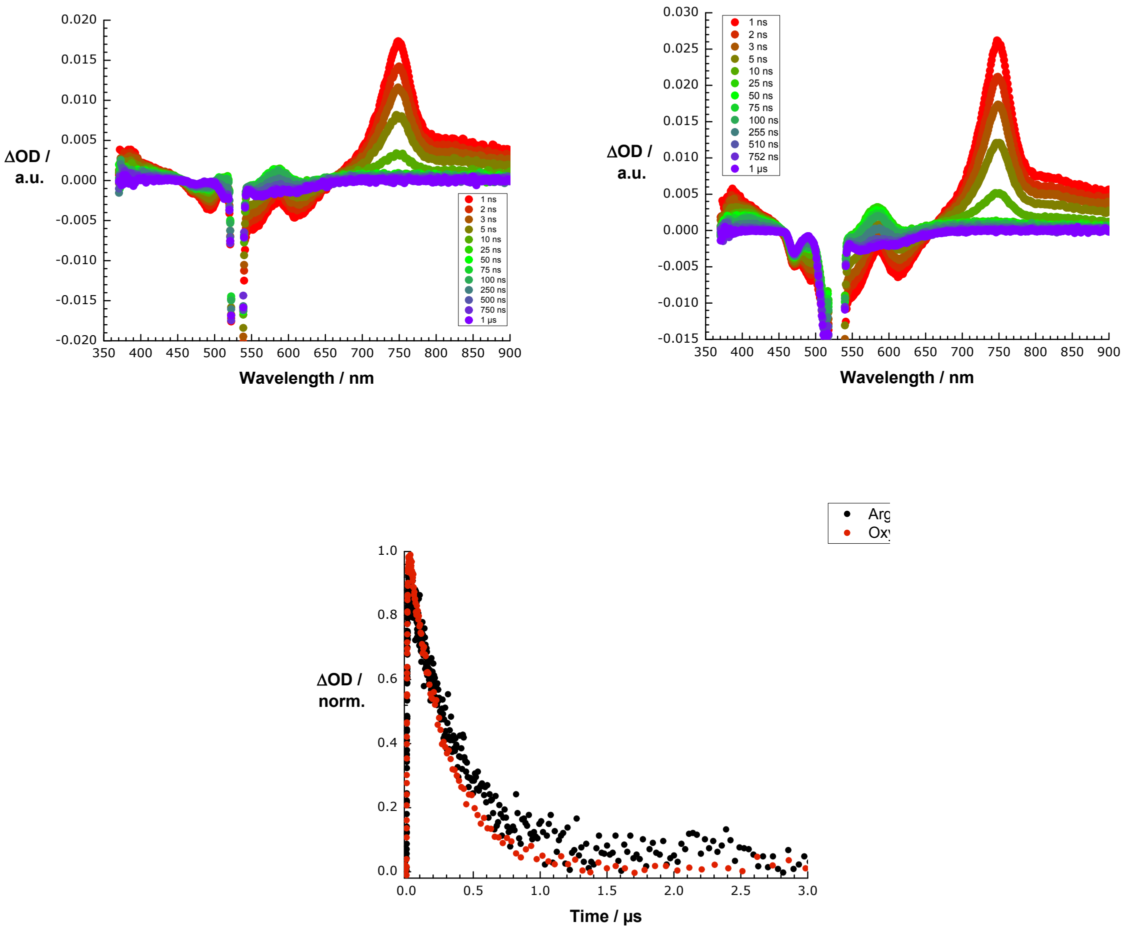

*Figure S33: Top left: : Differential absorption spectra of **1** (c=1x10^{-4} M) in H_2O in argon saturated atmosphere with different time delays from 1 (red) to 1000 ns (blue) obtained upon 530 nm laser excitation. Top right: Differential absorption spectra of **1** (c=1x10^{-4} M) in H_2O in oxygen saturated atmosphere with different time delays from 1 (red) to 1000 ns (blue) obtained upon 530 nm laser excitation. Bottom: Normalized time absorption profiles recorded at 585nm in the absence (black) and in the presence of molecular oxygen (red).*

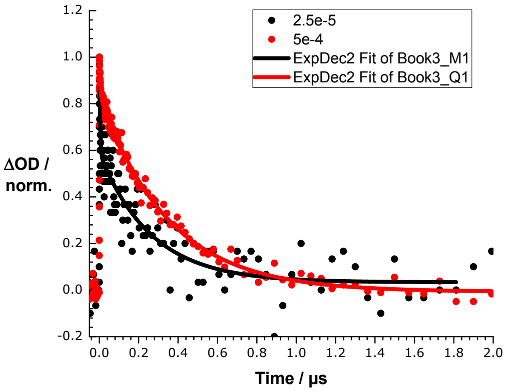

*Figure S34: Normalized time absorption profiles monitored at 420 nm with 2.5x10^{-5} M (black) and 5x10^{-4} M (red) of **1** in H_2O upon 530 nm laser excitation.*

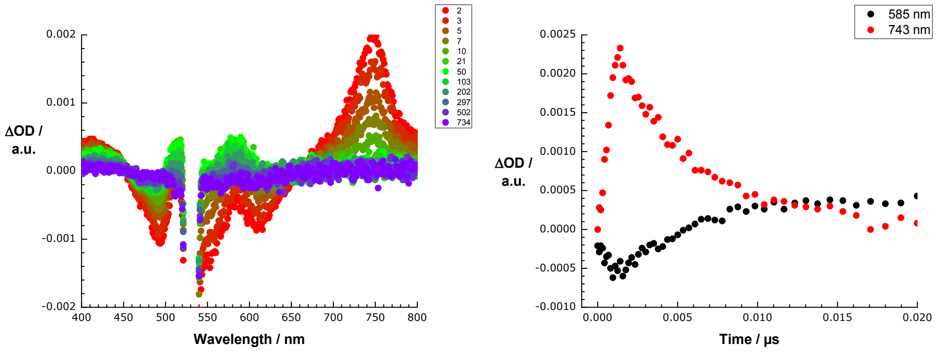

*Figure S35: Left: Differential absorption spectra of **1** (c=5x10^{-5} M) in H_2O with different time delays from 2 (red) to 753 ns (blue) obtained upon 530 nm laser excitation. Right: Time absorption profiles at 585 nm (black) and 743 nm (red) monitoring the excited state decay.*

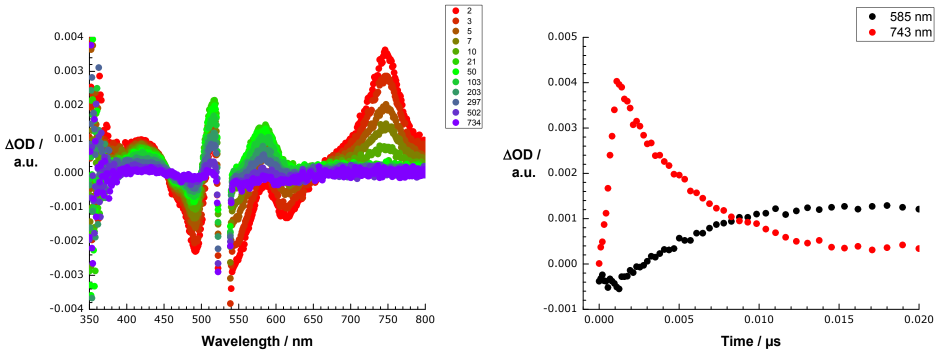

*Figure S36: Left: Differential absorption spectra of **1** (c=1x10^{-4} M) in H_2O with different time delays from 2 (red) to 753 ns (blue) obtained upon 530 nm laser excitation. Right: Time absorption profiles at 585 nm (black) and 743 nm (red) monitoring the excited state decay.*

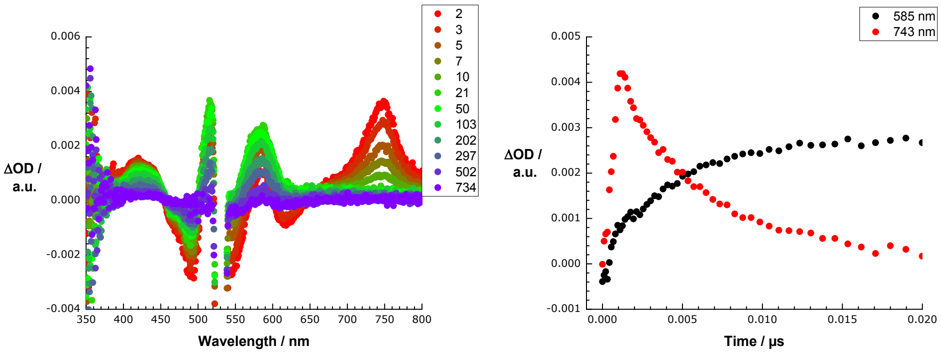

Figure S37: Left: Differential absorption spectra of ***1*** *($c=2.5x10^{-4}$ M) in H_2O with different time delays from 2 (red) to 753 ns (blue) obtained upon 530 nm laser excitation. Right: Time absorption profiles at 585 nm (black) and 743 nm (red) monitoring the excited state decay.*

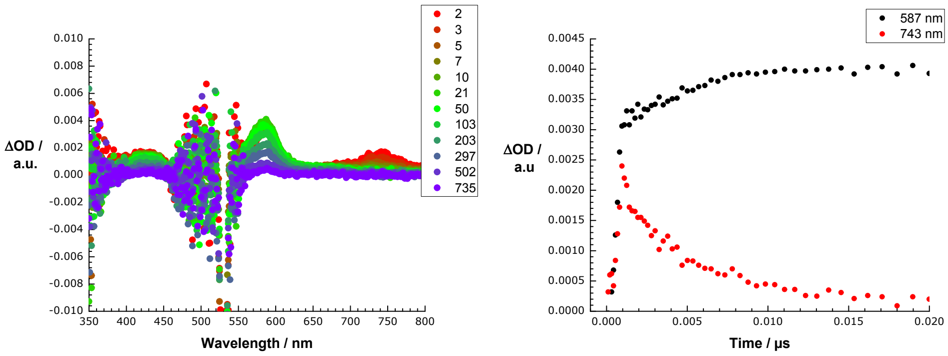

*Figure S38: Left: Differential absorption spectra of **1** (c=1x10^{-3} M) in H_2O with different time delays from 2 (red) to 753 ns (blue) obtained upon 530 nm laser excitation. Right: Time absorption profiles at 585 nm (black) and 743 nm (red) monitoring the excited state decay.*

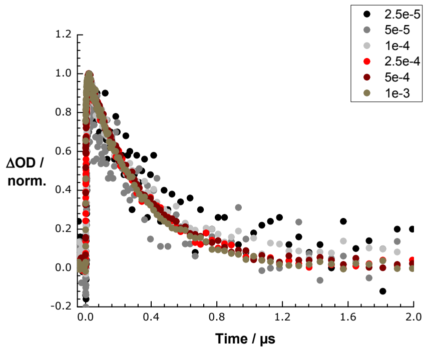

*Figure S39: Normalized time absorption profiles monitored at 585 nm with c = 2.5×10^{-5} (black) , 5×10^{-5}(dark grey), 1×10^{-4}(grey) , 2.5×10^{-4} (red), 5×10^{-4}(brown), 1×10^{-3}M (light brown) of **1**.*

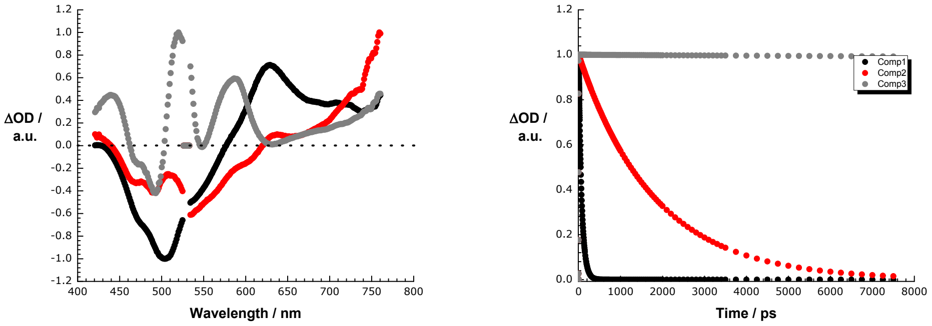

*Figure S40: Left: Normalized evolution associated spectra (nEAS) of **1** in H_2O (c = 5 x 10^{-4} M) on the pico- and nanosecond time scale as obtained from global analysis showing the normalized EAS of aggregate centered excited states (black), the resulting triplet excited states (grey) and the singlet excited states in monomeric **1** (red). Right: Concentration-time profiles corresponding to the spectra shown on the left.*

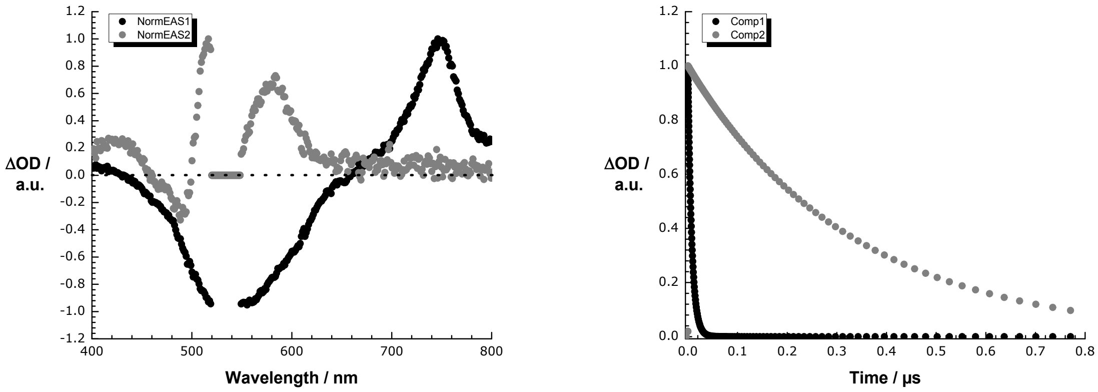

*Figure S41: Left: Normalized evolution associated spectra (nEAS) of **1** in H_2O ($c = 5 \times 10^{-4}$ M) on the nanosecond time scale as obtained from global analysis showing the normalized EAS of singlet excited states (black) and triplet excited states (grey) in aggregated **1**. Right: Concentration-time profiles corresponding to the spectra shown on the left.*

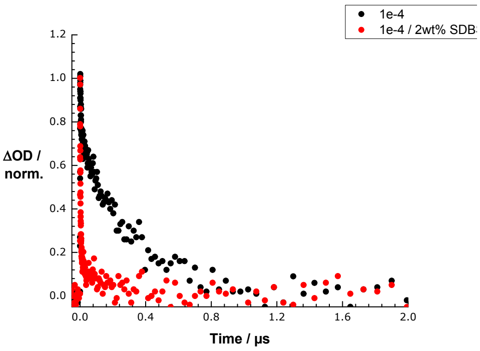

Figure S42: Normalized time absorption profiles of ***1*** *(black) and* ***1****/SDBS (red) monitored at 420 nm in* H_2O*. c(****1****) = 1x10*$^{-4}$*M.*

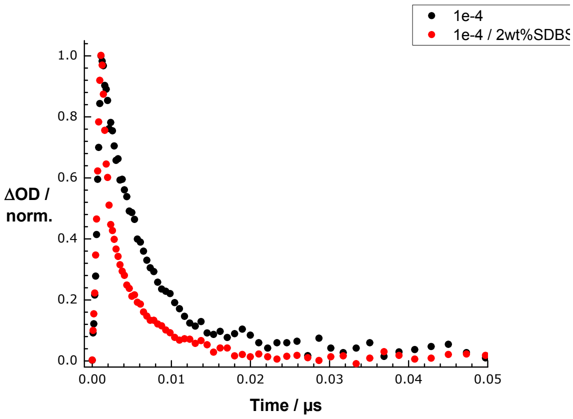

*Figure S43: Normalized time absorption profiles of **1** (black) and **1**/SDBS (red) monitored at 740 nm in* H_2O*. c(**1**) = 1x10*$^{-4}$*M.*

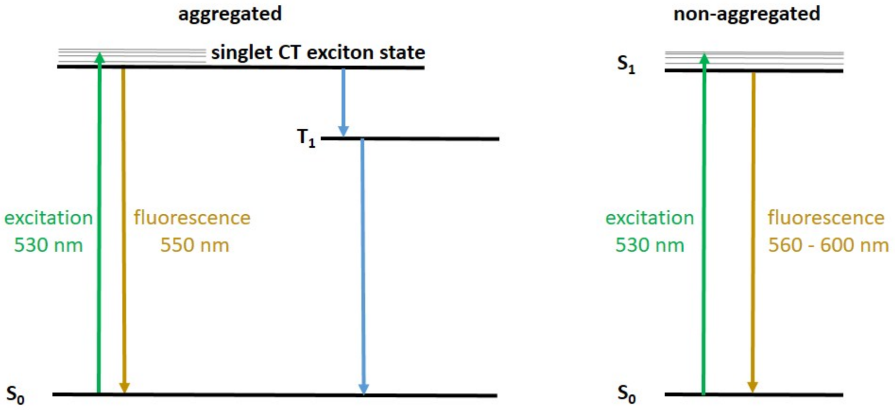

Figure S44: schematic representation of the deactivation channels in aggregated and non- aggregated solution of ***1****.*

6. Non-brominated reference PDI

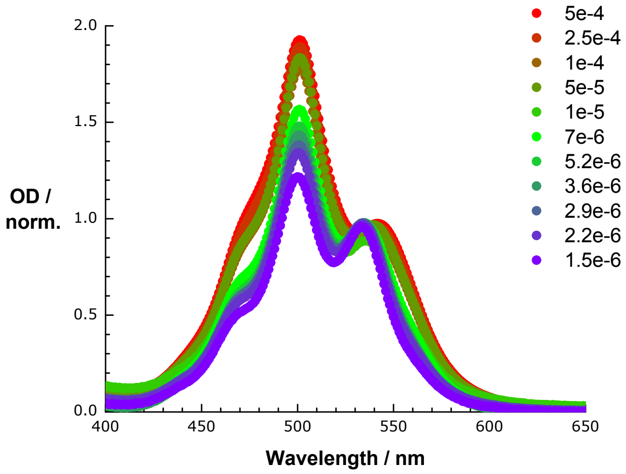

Figure S45: Normalized absorption of a non brominated reference PDI with different concentrations from 1x10^{-6} *M (blue) to 5x*10^{-4} *M (red) recorded in* H_2O.

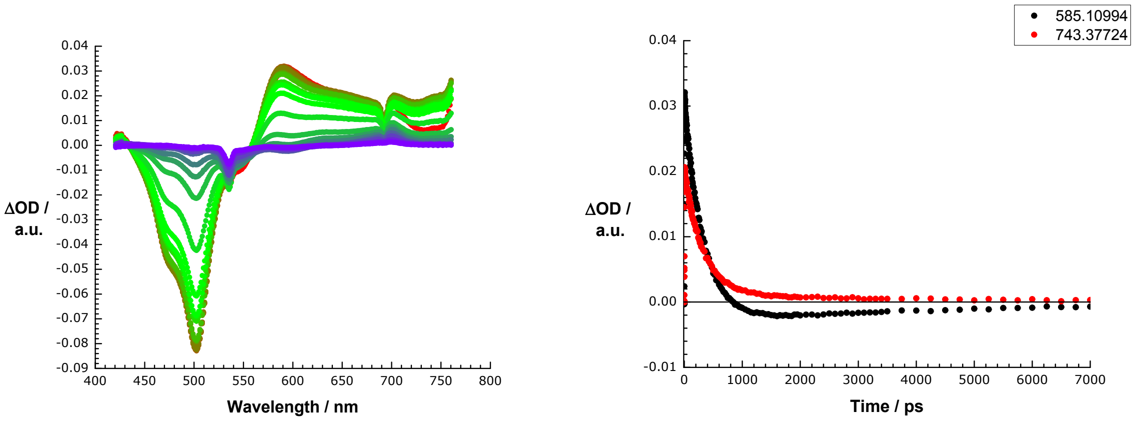

Figure S46: Left: Differential absorption spectra of a non-brominated reference PDI (c=1x10 $^{-4}$ M) in H_2O with different time delays from 2 (red) to 7500 ps (blue) obtained upon 530 nm laser excitation. Right: Time absorption profiles at 585 nm (black) and 750 nm (red) monitoring the excited state decay.

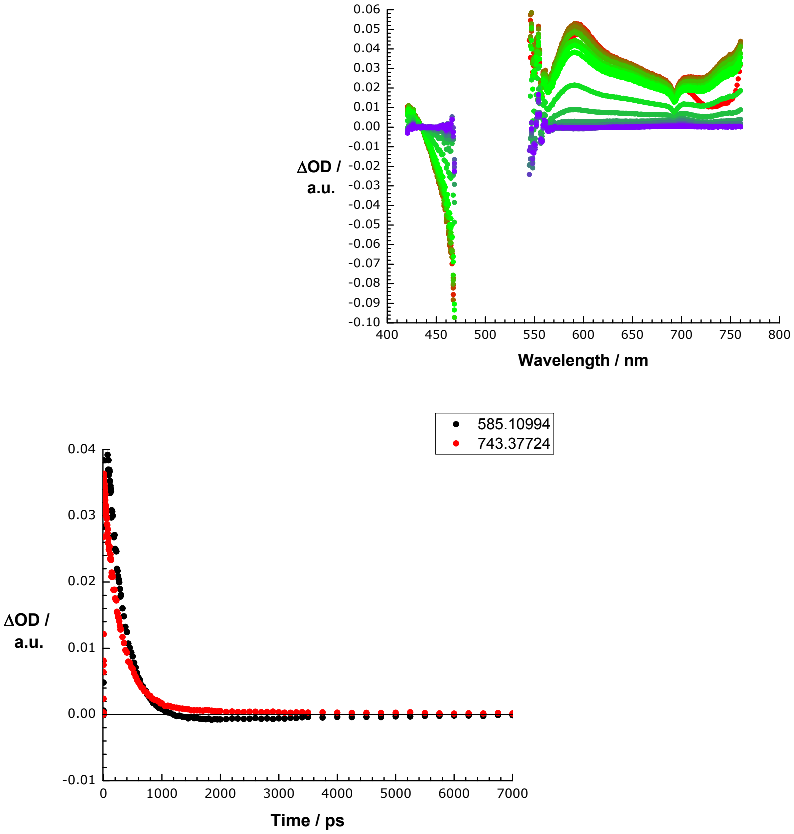

Figure S47: Left: Differential absorption spectra of a non-brominated reference PDI (c=1x10^{-3} M) in H_2O with different time delays from 2 (red) to 7500 ps (blue) obtained upon 530 nm laser excitation. Right: Time absorption profiles at 585 nm (black) and 750 nm (red) monitoring the excited state decay.

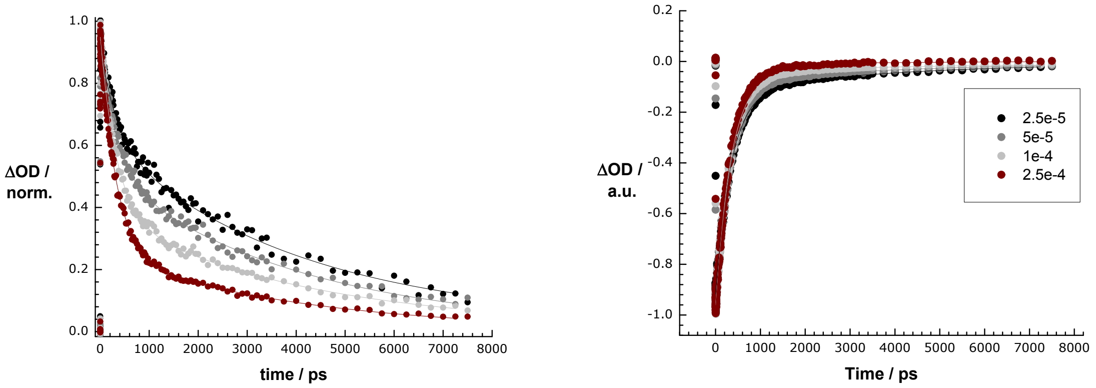

Figure S48: Normalized time absorption profiles monitored at 700 nm (left) and 500 nm (right) with 2.5x10^{-5} M (black) and 2.5x10^{-4} M (red) of the reference PDI in H$_2$O upon 530 nm laser excitation.

7. Temperature dependent measurements

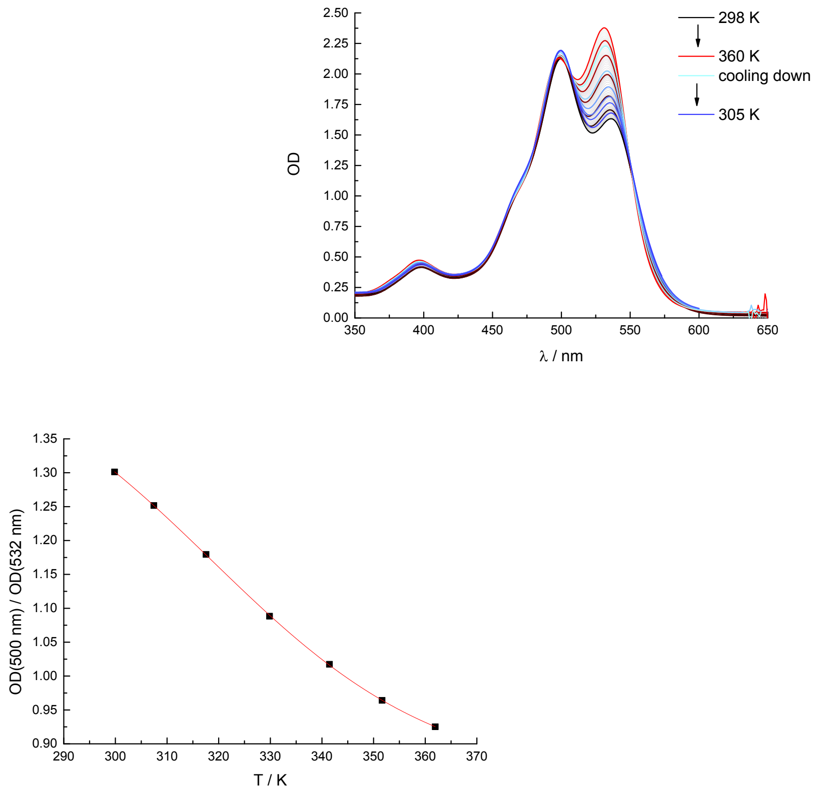

Figure S49: left: Temperature dependent absorption spectra of 1 (c=1x10^4 M) in H$_2$O. Heating from 298 K to 360 K (black to red) and cooling down to 305 K (light blue to blue). right: Ratio of the optical density at 500 nm and optical density at 532 nm in dependence of the temperature – measured during the heating cycle. Boltzmann fit in red, inflection point at 318 K.

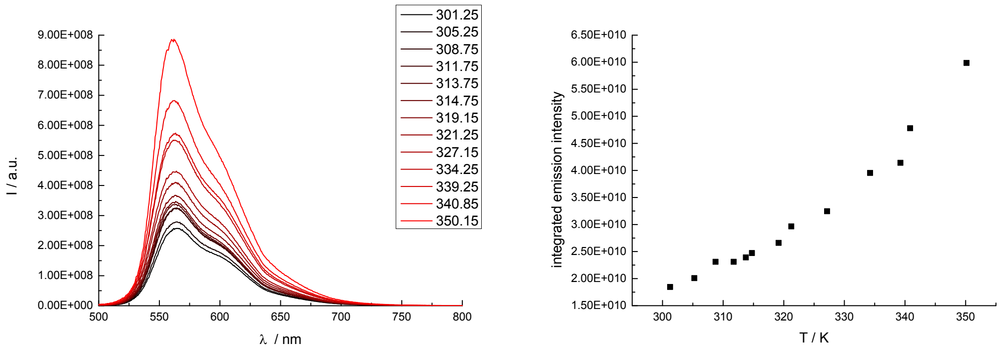

Figure S50: left: Temperature dependent emission spectra of 1 (c=1x10^4 M) in H_2O. Heating from 301 K to 350 K (black to red). right: Integrated emission intensity in dependence of applied temperature – measured during the heating cycle.

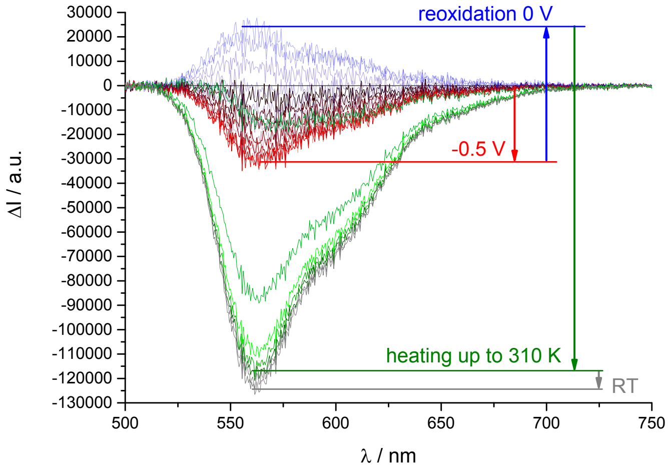

Figure S51: Differential changes in fluorescence of ***1*** *(1.0 x 10^{-4} M, H_2O, 0.05 M Na_2SO_4) throughout one spectroelectrochemical cycle (0 mV – (-500 mV) – 0 mV, vs Ag-wire as quasi reference electrode at room temperature. Reduction is shown from black to red, reoxidation is shown in blue. After the reoxidation the sample was heated to 310 K (green) and cooled down to roomtemperature (RT, grey).*

8. References

---

[i] D.A. Case, D.S. Cerutti, T.E. Cheatham, III, T.A. Darden, R.E. Duke, T.J. Giese, H. Gohlke, A.W. Goetz, D. Greene, N. Homeyer, S. Izadi, A. Kovalenko, T.S. Lee, S. LeGrand, P. Li, C. Lin, J. Liu, T. Luchko, R. Luo, D. Mermelstein, K.M. Merz, G. Monard, H. Nguyen, I. Omelyan, A. Onufriev, F. Pan, R. Qi, D.R. Roe, A. Roitberg, C. Sagui, C.L. Simmerling, W.M. Botello-Smith, J. Swails, R.C. Walker, J. Wang, R.M. Wolf, X. Wu, L. Xiao, D.M. York and P.A. Kollman (2017), AMBER 2017, University of California, San Francisco.

[ii] W. L. Jorgensen, J. Chandrasekhar, J. D. Madura, R. W. Impey, and M. L. Klein, Comparison of simple potential functions for simulating liquid water, J. Chem. Phys. 79 (1983) 926-935

[iii] Wang, J., Wolf, R. M.; Caldwell, J. W.;Kollman, P. A.; Case, D. A. "Development and testing of a general AMBER force field". Journal of Computational Chemistry, 25, 2004, 1157-1174.